

LHC constraints on dark matter with (130 GeV) gamma ray lines

James M. Cline, Grace Dupuis, Zuwei Liu

Department of Physics, McGill University, 3600 Rue University, Montréal, Québec, Canada H3A 2T8

ABSTRACT: Dark matter annihilation into photons in our galaxy would constitute an exciting indirect signal of its existence, as underscored by tentative evidence for 130 GeV dark matter in Fermi/LAT data. Models that give a large annihilation cross section into photons typically require the dark matter to couple to, or be composed of, new charged particles, that can be produced in colliders. We consider the LHC constraints on some representative models of these types, including the signals of same-sign dileptons, opposite-sign dileptons, events mimicking the production and decay of excited leptons, four-photon events, resonant production of composite vectors decaying into two photons, and monophoton events.

Contents

1	Introduction	1
2	Theoretical models	2
2.1	Loop-mediated model	3
2.2	Magnetic dipole DM model	3
2.3	<i>s</i> -channel models	4
2.4	Dark glueballs	6
3	LHC production	6
4	Same-sign dileptons	7
5	Vector “meson” production	9
6	Excited electron/muon limits	11
7	Two- and four-photon events	12
7.1	Diphoton constraints	13
7.2	4-photon final state	13
8	Monophoton limits	16
9	Viability of 130 GeV (and other) DM models	18
9.1	Loop model	18
9.2	MDM Model	20
9.3	<i>s</i> -channel regime	21
9.4	Beyond 130 GeV	21
10	Conclusion	23
A	Amplitude for photoproduction of ϕ_s	25
B	“Bohr model” of exotic mesons	25

1 Introduction

The search for particle dark matter is being vigorously pursued from three complementary directions: direct detection by its scattering on nucleons, indirect signals from annihilation in the galaxy, and its production in colliders. Ideally, a positive detection of dark matter by one of these techniques would be corroborated by at least one of the others. Among the signatures amenable to indirect searches, dark matter annihilating into photons is interesting because of the sensitivity of experiments like the Fermi Large Area Telescope and the HESS II atmospheric Cherenkov telescope to the resulting gamma rays.

Indeed, there are hints that an excess of 130 GeV gamma rays possibly due to such annihilations are coming from the galactic center [1]-[8], and even from external clusters of galaxies [9] or from other sources within the galaxy [10].

A relatively large cross section $\sigma(\chi\chi \rightarrow \gamma\gamma) \sim 0.1\langle\sigma v\rangle_0$ is needed to explain the observation [2, 3], where $\langle\sigma v\rangle_0 \cong 1\text{pb}\cdot c$ is the canonical annihilation cross section needed to explain the observed relic density through thermal freeze-out. For dark matter with mass ~ 100 GeV, $\sim 0.1\langle\sigma v\rangle_0$ is also close to the upper limit placed by Fermi/LAT in ref. [11]. Fermi itself [8] finds a less significant excess at 130 GeV than previous authors (local significance of 3.3σ), concluding that “more data and study are needed to clarify the origin of this feature.” Suggestions that the bump is due to instrumental noise have been studied [12, 13], with the conclusion that such an origin is difficult to reconcile with the localization of the signal near the galactic center.

Most particle physics models of dark matter do not predict such a large value of $\sigma(\chi\chi \rightarrow \gamma\gamma)$, hence models that do so have been relatively less explored in terms of their complementary predictions for the LHC; see refs. [14]-[21] for existing studies along these lines. In the present work we consider the implications for LHC of two classes of models that have been proposed for the 130 GeV line(s): one in which scalar dark matter χ couples to a new charge-2 scalar S , that mediates $\chi\chi \rightarrow \gamma\gamma$ through an S loop [22, 23]¹ and the other in which dark matter is a partially composite fermion with a large magnetic moment, inherited from its charged constituents [25, 26]. Both models involve new charged particles that transform under a hidden-sector confining gauge group SU(2) or SU(3), and so they share some common predictions, such as the production of SS^* pairs that “hadronize” and decay into pairs of photons, leading to distinctive 4-photon events. Another common prediction is that exotic charged bound states should be pair-produced and decay into exotic final states, either like-sign lepton pairs or lepton-photon pairs. Neutral bound states can also be produced singly as a resonance in the s -channel analogous to J/ψ , with decays into fermion pairs. There are the more familiar monophoton constraints coming from initial state radiation in the case where the resonantly produced state decays into dark matter pairs. In addition we find a novel source of monophotons coming from the radiative decay of “vector mesons” of the new SU(N) into their spin-0 ground states.

These classes of dark matter models that are capable of significant $\chi\chi \rightarrow \gamma\gamma$ annihilation thus lead to a number of low-background signatures for LHC, and we wish to characterize the extent to which LHC can constrain such models when the cross section $\sigma(\chi\chi \rightarrow \gamma\gamma)$ is close to constraints from Fermi/LAT observations. We start in section 2 with a review of the models considered, and estimates of their respective cross sections for annihilation into monoenergetic photons at the galactic center. We compute the cross section for LHC production of charged scalar pairs as a function of energy in sect. 3. This is followed by an analysis of LHC constraints on the models from the processes of decays of doubly-charged scalars into same-sign leptons (sect. 4), direct production of vector “mesons” decaying to leptons (sect. 5), decays of singly-charged composite fermions into lepton plus photon (sect. 6), decays of neutral composite states to diphotons and diphoton pairs (sect. 7), and monophoton events (sect. 8). We synthesize these constraints to give an overview of the viability for the models to explain 130 GeV gamma rays (as well a generalizations to masses of other possible future DM candidates) in sect. 9 and summarize our findings in sect. 10.

2 Theoretical models

In this section we summarize the three classes of models that motivated this study, focusing on their predictions for γ -ray lines from dark matter annihilation. All of them involve a new confining $SU(N_c)_d$

¹for a similar model in which vector dark matter couples to charged fermions, see [24].

gauge group (with subscript d for “dark”) and electrically charged scalar particles S that transform in the fundamental of $SU(N_c)_d$.

2.1 Loop-mediated model

In the first class of models, the dark matter is assumed to be a scalar, with coupling $(\lambda_{S\chi}/2)\chi^2|S|^2$ to the new charged scalar S . The annihilation $\chi\chi \rightarrow \gamma\gamma$ is mediated by a loop of S . To get a large enough cross section to be relevant for current γ -ray observations, the loop-suppression of the amplitude should be overcome by a somewhat large electric charge $q_s \geq 2$, and the color multiplicity N_c of S . In ref. [22], the interaction potential between χ , S and the Higgs boson H was considered to be

$$V_{\text{int}} = \frac{\lambda_{S\chi}}{2}\chi^2|S|^2 + \lambda_{Hs}|H|^2|S|^2 + \frac{\lambda_{H\chi}}{2}\chi^2|H|^2 \quad (2.1)$$

It was shown that a cross section for $\chi\chi \rightarrow \gamma\gamma$ consistent with the value determined in ref. [2] for 130 GeV dark matter could be obtained for parameter values $q_s = 2$, $\lambda_{S\chi} = 3$, $N_c = 3$, $m_s = 170$ GeV, for example. More generally, one can express the cross section $\langle\sigma v\rangle_{\chi\chi \rightarrow \gamma\gamma}$ in terms of the mass ratio $r = m_s/m_\chi$ as

$$\frac{\langle\sigma v\rangle_{\chi\chi \rightarrow \gamma\gamma}}{0.1\langle\sigma v\rangle_0} = 0.44 \left(\frac{q_s}{2}\right)^4 \left(\frac{\lambda_{S\chi}}{3}\right)^2 \left(\frac{N_c}{3}\right)^2 \left(\frac{m_\chi}{130 \text{ GeV}}\right)^{-2} r^{-4} f(r) \quad (2.2)$$

where $f(r) = 9r^4(1 - r^2(\sin^{-1}(1/r))^2)^2 \rightarrow 1$ for large r and is numerically fit by the formula $f(r) \cong 1 + 0.4/(r - 0.972)$ which is good to 6% for any value of $r > 1.001$. (We define f in this way so that the r dependence in (2.2) is all transparently in the r^{-4} factor for $r \gg 1$.) The combination $r^{-4}f(r)$ reaches its maximum value $\cong 19.4$ when $r = 1$. Recall that $\langle\sigma v\rangle_0 = 1 \text{ pb}\cdot\text{c}$ is the nominal relic density cross section.

In order to avoid the problem of charged relics (namely the “baryon” made from a bound state of N_c S constituents) it is necessary to introduce a neutral fundamental field T , which is also taken to be scalar. If T is lighter than S , then the decay $S \rightarrow Tee$ can be mediated by the dimension-5 operator $\Lambda^{-1}ST^*\bar{e}_R^c e_R$. In general one could have couplings to any right-handed leptons, $\Lambda_{ij}^{-1}ST^*\bar{l}_{R,i}^c l_{R,j}$. These couplings are constrained by LHC searches for like-sign lepton pairs, as we will discuss in section 4. Below the dark confinement scale Λ_d , the dimension-5 operator will evolve to a renormalizable Yukawa interaction $\eta_{sT}\bar{e}_R^c e_R$ with coupling of order Λ_d/Λ . The charged η_{sT} will decay before big bang nucleosynthesis (where its presence would change primordial abundances) as long as $\Lambda \lesssim 10^{16.5}(\Lambda_d/100 \text{ GeV})^{3/2} \text{ GeV}$.

2.2 Magnetic dipole DM model

In the second class of models, dark matter is a mixture of an elementary fermion and a composite one made from charged constituents, that can give a large transition magnetic moment $\frac{1}{2}\mu_{12}\bar{\chi}_1\sigma_{\mu\nu}F^{\mu\nu}\chi_2$ between the dark matter χ_1 and an excited state χ_2 [25]. We refer to these as magnetic dark matter (MDM) models. The charged constituents are a fermion ψ and boson S that transform in the fundamental of the $SU(N_c)_d$ gauge symmetry. In the simplest case, $N_c = 2$. The charges of ψ and S are constrained by the prohibition on stable charged relics, which in the confining $N_c = 2$ theory would be the lightest of the “baryonic” bound states SS , $\psi\psi$ and $S^*\psi$ (we take S and ψ to have opposite charges). It is sufficient to introduce a renormalizable operator $\epsilon_{ab}S_a^*\bar{l}_R\psi_b$ that leads to mass mixing of $S^*\psi$ with the standard model lepton l_R , hence to decays of the would-be charged relic into l_R and

photon or dark matter. This shows that S and ψ should have charges $\pm 1/2$.² Since we take them to be singlets under $SU(2)_L$, they have hypercharge ± 1 .

If the excited dark matter state χ_2 is abundant in the early universe, when DM annihilations are freezing out to fix the relic abundance n_χ , the magnetic-moment induced process $\chi_1\chi_2 \rightarrow \gamma^* \rightarrow f\bar{f}$ (where f represents standard model fermions) is so efficient as to suppress n_χ below the value needed for χ_1 to account for full dark matter density of the universe, leading to an insufficient rate for $\chi_1\chi_1 \rightarrow \gamma\gamma$ in the galaxy. This can be avoided by arranging for $m_{\chi_2} - m_{\chi_1} \gtrsim 10$ GeV. In ref. [25] it was noted that for a range of magnetic moment values μ_{12} , annihilations $\chi_1\chi_1 \rightarrow \gamma\gamma$, through the process of fig. 1(a), can have a cross section that is larger than $\langle\sigma v\rangle_0$, so that n_χ is again suppressed relative to the canonical value n_0 , but that the γ -ray signal in the galaxy is nevertheless at the observed level. Because n_χ scales as $1/\langle\sigma v\rangle$, we find that the effective value of the cross section, as constrained by searches for gamma ray lines, goes inversely to the actual cross section:

$$\langle\sigma v\rangle_{\text{eff}} = \frac{\langle\sigma v\rangle_0^2}{\langle\sigma v\rangle} \cong (0.04 - 0.1)\langle\sigma v\rangle_0 \quad (2.3)$$

The range 0.04–0.1 corresponds to the values estimated for the tentative 130 GeV γ -ray signal by refs. [2] and [3]. In ref. [25] it was shown that this range of cross sections corresponds to magnetic moments in the interval $1.6 < \mu_{12} \cdot \text{TeV}/f(r) < 2$ where $r = m_{\chi_2}/m_{\chi_1} > 1$ and $f(r) = \sqrt{(r^{-1} + r)}/2 \geq 1$. Note that $\langle\sigma v\rangle$ scales as μ_{12}^4 .

In this model, the dark matter gets its magnetic moment from the bound state $\eta \equiv S\psi$, whose magnetic moment is estimated as that of the fermionic constituent ψ , $\mu_\eta = e/(2m_\psi)$, in analogy to the magnetic moments of baryons in the quark model. The DM mass eigenstates are mixtures of a Majorana fermion and the composite Dirac state η , and there is some reduction of μ_{12} relative to μ_η by a mixing angle θ : $\mu_{12} = \cos\theta \mu_\eta$. Ref. [25] (see fig. 3) found that $1/\sqrt{2} \leq \cos\theta \leq 1$ for the cases of interest. Taking $2m_\psi \sim 130$ GeV, this gives μ_{12} roughly consistent with the desired range mentioned above.

Putting the above results together, we find that the effective cross section as would be inferred by γ -ray observations is predicted to be

$$\langle\sigma v\rangle_{\text{eff}} \cong 0.1 \langle\sigma v\rangle_0 \left(\frac{f(r)}{\cos\theta}\right)^4 \left(\frac{m_\psi}{100 \text{ GeV}}\right)^4 \quad (2.4)$$

This prediction is only valid for $\langle\sigma v\rangle_{\text{eff}} \leq \langle\sigma v\rangle_0$ since if this condition is violated, it means that the dark matter density is larger than allowed by observations such those of [27]. The estimate (2.4) however assumes that there is no other annihilation channel besides $\chi_1\chi_1 \rightarrow \gamma\gamma$ mediated by the magnetic moment interaction. In fact, this model also has the possibility of strong $\chi\chi \rightarrow \gamma\gamma$ annihilation through the channel shown in fig. 1(b). This diagram must be subdominant to that of fig. 1(a) in order to justify the estimate (2.4). In ref. [25] it was argued that this is true as long as the s -channel diagrams are not resonantly enhanced. But the other case is an interesting possibility in itself, which can in fact also be incorporated in the loop-mediated model. We consider these s -channel models next.

2.3 s -channel models

A third generic mechanism for producing γ rays is for DM to annihilate, possibly resonantly, into an intermediate particle η that subsequently decays into two photons as shown in fig. 1(b). A natural

²One can admit larger charges $\pm(n + 1/2)$ by using higher-dimensional operators $\epsilon_{ab} S_a^* \bar{l}_R \psi_b (\bar{l}_R l_R^c / \Lambda^3)^n$ to induce the charged relic decays. Here we assume the simplest possibility $n = 0$.

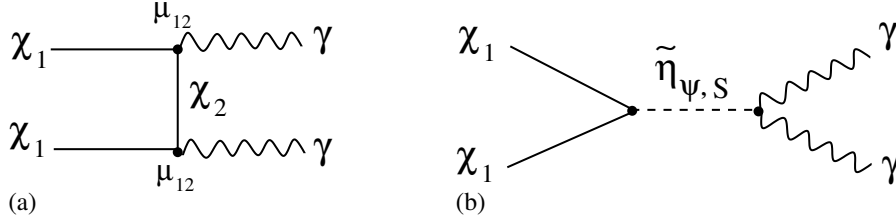


Figure 1. Annihilation of dark matter into photons by (a) magnetic moment interaction and (b) s -channel exchange of the bound states $\eta_s = S^*S$ or $\eta_\psi = \bar{\psi}\psi$.

realization of this idea is for η to be a bound state of a charged particle-antiparticle pair, analogous to the η meson of QCD; the decay $\eta \rightarrow \gamma\gamma$ is then inevitable. This scenario can be achieved in either of the models presented above by an appropriate choice of parameters.

In the “loop model,” there is an enhancement in the limit $m_S \rightarrow m_\chi$, which kinematically coincides with the picture where a bound state $\eta_s = S^*S$ is resonantly produced and subsequently decays to photons. In the strongly interacting description, we can identify $S^*S = f_\eta \eta_s$ where f_η is a decay constant of order the confinement scale, such that $\langle \eta_s | S^*S | 0 \rangle = f_\eta$. The quartic coupling $\chi^2 |S|^2$ then becomes a cubic interaction $(\lambda_{S\chi}/2) f_\eta \eta_s \chi^2$. By comparing to the theory of η and π^0 decays in QCD, we can estimate the coupling of η_s to photons as

$$\alpha \frac{q_s^2 N_c}{4\pi f_\eta} \eta_s F_{\mu\nu} F^{\mu\nu} \quad (2.5)$$

where we have taken η_s to be even under parity and hence used F^2 rather than $F\tilde{F}$. Although this result is adapted from the anomaly of the axial current for fermionic constituents, we will assume that a similar result holds for the present case of bosonic constituents. The partial width for $\eta_s \rightarrow \gamma\gamma$ is then

$$\Gamma_{\eta_s \rightarrow \gamma\gamma} = \frac{\alpha^2 N_c^2 q_s^4}{64\pi^3 f_\eta^2} m_\eta^3 \quad (2.6)$$

which is 4 MeV for the parameter choices $q_s = 2$, $N_c = 3$, $m_\eta = 260$ GeV, $f_\eta = 130$ GeV for example. The width for $\eta_s \rightarrow \chi\chi$ is

$$\Gamma_{\eta \rightarrow \chi\chi} = \frac{\lambda_{S\chi}^2 f_\eta^2}{16\pi m_\eta} \sqrt{1 - 4m_\chi^2/m_\eta^2} \quad (2.7)$$

This is generically much larger than $\Gamma_{\eta \rightarrow \gamma\gamma}$, unless the former is kinematically forbidden. The cross section for $\chi\chi \rightarrow \gamma\gamma$ corresponding to fig. 1(b) is

$$\langle \sigma v \rangle_{\chi\chi \rightarrow \gamma\gamma} = \frac{\alpha^2 \lambda_{S\chi}^2 N_c^2 q_s^4 m_\chi^2}{32\pi^3 ((4m_\chi^2 - m_\eta^2)^2 + \Gamma^2 m_\eta^2)} \quad (2.8)$$

Defining $\Delta r = m_{\eta_s}^2/4m_\chi^2 - 1$ and assuming $|\Delta r| \gg \Gamma m_{\eta_s}/4m_\chi^2$, we find that

$$\frac{\langle \sigma v \rangle_{\chi\chi \rightarrow \gamma\gamma}}{0.1 \langle \sigma v \rangle_0} = \left(\frac{q_s}{2}\right)^4 \left(\frac{\lambda_{S\chi}}{3}\right)^2 \left(\frac{N_c}{3}\right)^2 \left(\frac{m_\chi}{130 \text{ GeV}}\right)^{-2} \frac{0.9}{(\Delta r)^2} \quad (2.9)$$

This is roughly consistent with (2.4), showing that we can obtain a similar estimate from the perturbative loop calculation as from the bound state picture. In both cases, the annihilation cross section becomes enhanced relative to the generic value when m_η is close to $2m_\chi$.

For the MDM model of section 2.2, the dark matter is fermionic, and the interaction $g\bar{\chi}\eta_s\chi$ has dimension 4; the coupling $\lambda_{S\chi}$ in (2.9) should be replaced by the Yukawa coupling g . This interaction is generated by strong dynamics, unsuppressed by any flavor symmetries, because the χ states contain $S\psi$ or $S^*\bar{\psi}$ constituents, which have a large overlap with η_s or η_ψ via the annihilation of the extra $\psi\bar{\psi}$ or SS^* pair. g is therefore analogous to the pion-nucleon coupling which is known to be large, $g \sim 14$ (see for example [28]). This can compensate the suppression of 256 relative to the loop model, from the smaller charge $q_s = 1/2$, and a further suppression of 2.25 from the smaller value of N_c . To overcome these factors, one needs to be somewhat close to resonance, with $\Delta r = 0.2$, thus requiring a tuning of $m_\eta/2m_\chi$ at the level of 10%.

2.4 Dark glueballs

In the following analysis, glueballs of the hidden $SU(N)_d$, which we denote by θ , could play an important role because they might be the lightest ‘‘hadrons’’ of the hidden sector, if the confinement scale Λ_d is lower than the mass of the colored constituents. In QCD, there exist candidate glueball states with mass around 1370 and 1700 MeV [29]. In our models, the lightest glueball mass $m_\theta \sim \Lambda_d$ cannot be less than the dark matter mass; otherwise the annihilation channel $\chi\chi \rightarrow \theta\theta$ would strongly suppress the DM relic density.

In these models, the main decay channel of the glueball is into two photons, mediated by a loop of the charged constituent. Thus the lightest glueball could be a Higgs boson imposter from the perspective of the $h \rightarrow \gamma\gamma$ channel. However if we take m_θ to be greater than the constituent masses, the production of glueballs from the decays of bound states will be kinematically forbidden. This removes one of the competing decay channels that would reduce the branching ratio of the bound states into two photons, which is of interest for constraining production of pairs of bound states, as we discuss in sect. 7.

3 LHC production

We begin our study of LHC constraints by computing the production cross section for $pp \rightarrow S^*S$ ($\psi\bar{\psi}$), where S (ψ) is the new charged scalar (fermion) that is taken to be neutral under $SU(2)_L$. The relevant interaction Lagrangian, including the standard model couplings to fermions, is given by

$$\mathcal{L}_{\text{int}} = -ieq_s(A_\mu - t_W Z_\mu)S^\dagger \overleftrightarrow{\partial}^\mu S - eq_f \bar{f} \gamma^\mu f A_\mu + e\bar{f} \gamma^\mu (\alpha_f + \beta_f \gamma_5) f Z_\mu \quad (3.1)$$

where q_s is the electric charge of S , $A \overleftrightarrow{\partial}_\mu B \equiv A\partial_\mu B - (\partial_\mu A)B$, $t_W \equiv \tan \theta_W$ (θ_W is the Weinberg angle), q_f is the electric charge of fermion f , and α_f (β_f) is its vector (axial-vector) coupling. For up quarks, $\alpha_u = -5t_W/12 + c_W/4$, $\beta_u = -(t_W + c_W)/4$, and for down quarks, $\alpha_d = t_W/12 - c_W/4$, $\beta_d = (t_W + c_W)/4$, where $c_W \equiv \cos \theta_W$.

The parton level cross section for the process ($q\bar{q} \rightarrow \gamma/Z \rightarrow S\bar{S}$) is

$$\begin{aligned} \hat{\sigma}(q\bar{q} \rightarrow S\bar{S}) &= \frac{N_c}{N_q} \frac{\beta^3}{4} \left(\frac{4\pi\alpha^2}{3\hat{s}} \right) \\ &\times \left[q_s^2 q_q^2 + \frac{q_s^2 t_W^2 (\alpha_q^2 + \beta_q^2) \hat{s}^2}{(\hat{s} - m_Z^2)^2 + m_Z^2 \Gamma_Z^2} + \frac{2q_s^2 t_W q_q \alpha_q (\hat{s} - m_Z^2) \hat{s}}{(\hat{s} - m_Z^2)^2 + m_Z^2 \Gamma_Z^2} \right] \end{aligned} \quad (3.2)$$

where \hat{s} is the square of center-of-mass energy in the parton level, $\beta = \sqrt{1 - 4m_S^2/\hat{s}}$, $N_q = 3$ is the QCD color factor, N_c is the hidden sector color factor of the S -scalar, m_Z (Γ_Z) is the mass (decay

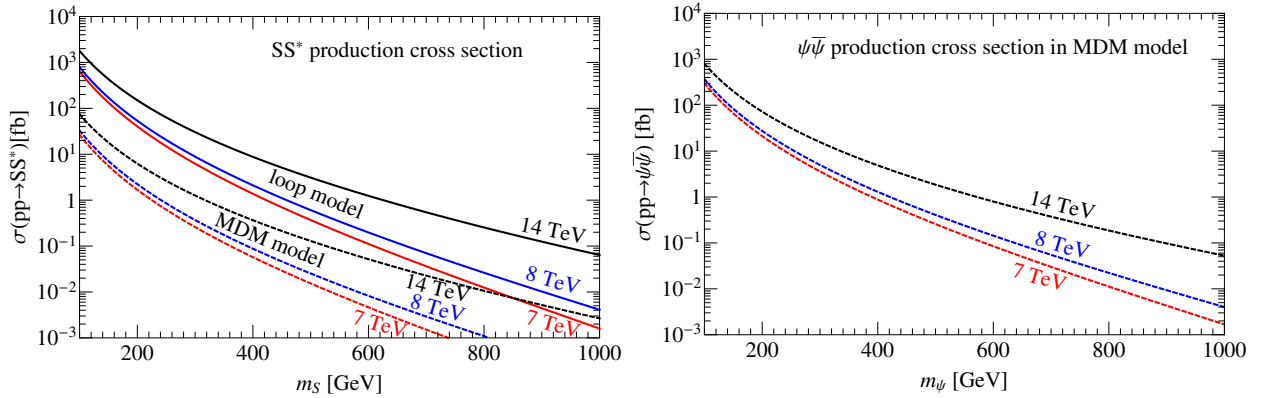


Figure 2. Left: the LHC production cross section of the charged scalar pair as a function of the scalar mass, m_S , for three different collider energies: 7, 8, and 14 TeV. Solid lines are for loop model with $q_s = 2$, $N_c = 3$, while dashed ones are for magnetic model with $q_s = 1/2$, $N_c = 2$. Right: same for production of fermion pairs $\psi\bar{\psi}$ in MDM model.

width) of the Z boson. For the analogous production of fermion pairs $\psi\bar{\psi}$, the factor of $\beta^3/4$ in (3.2) is replaced by $\beta(1 + 2m_s^2/\hat{s})$.

The hadronic cross section ($pp \rightarrow \gamma/Z \rightarrow S\bar{S}$) at LHC is

$$\frac{d\sigma(pp \rightarrow S\bar{S})}{dM_{S\bar{S}}} = K \frac{4M_{S\bar{S}}}{s} \sum_q \hat{\sigma}_{q\bar{q}}|_{\hat{s}=M_{S\bar{S}}^2} \int_{\tau}^1 \frac{dx}{x} q(x) \bar{q}(\tau/x) \quad (3.3)$$

where $\sqrt{s} = 7, 8, 14$ TeV are the LHC energies considered for our study, $\hat{\sigma}_{q\bar{q}} \equiv \hat{\sigma}(q\bar{q} \rightarrow S\bar{S})$ is the parton level cross section given in eq. (3.2), $M_{S\bar{S}}$ is the invariant mass of the scalar pair $S\bar{S}$, $\tau = M_{S\bar{S}}^2/s$, and $q(x)$ and $\bar{q}(x)$ are the parton distribution functions of quark q and \bar{q} with momentum fraction x . Here we also use the K -factor to take into account the NLO QCD corrections. For our purpose, we take $K \simeq 1.3$ [30]. Eq. (3.3) also applies for production of fermion pairs with the obvious substitution $S\bar{S} \rightarrow \psi\bar{\psi}$.

The total LHC production cross section for the scalar or fermion pairs is plotted in Fig. 2. Values of the charges q_s , q_ψ ; and gauge group rank N_c corresponding respectively to the loop and MDM models described above are adopted there.

4 Same-sign dileptons

Same-sign dilepton events can be produced at the LHC from the decay of the doubly charged scalars S that are present in the loop model. Recall that in order to avoid charged relics, this model introduces a dimension 5 operator $\Lambda_{ij}^{-1} T^* S \bar{\ell}_i^c \ell_j$ (where i, j are flavor indices of the right-handed leptons ℓ_i) to permit such decays, with T being a lighter electrically neutral scalar, also a fundamental of the $SU(N)_d$. Since the $SU(N)_d$ interactions are confining, the $S\bar{S}$ pairs produced as shown in fig. 3 will hadronize, in this case into spin-0, charge-2 bound states of S and T^* which we denote by η_{ST} .

CMS and ATLAS have placed upper limits on the cross section for production of like-sign dilepton final states [31, 32]. We have applied these to the loop model and derived the resulting constraints as

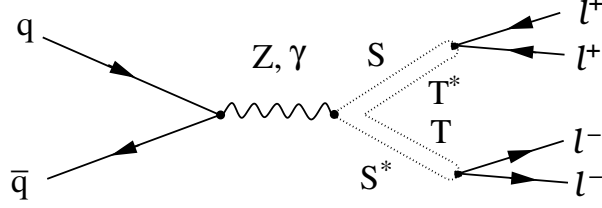


Figure 3. Production of η_{ST} pairs leading to like-sign dilepton events.

a function of the hidden meson mass $m_{\eta_{ST}}$, assuming that the dominant decays are into either ee , $\mu\mu$ or $\tau\tau$ final states. The resulting exclusion curves are plotted in Fig. 4. The model does not specify the flavor-dependence of the branching ratios, but it may be natural to assume, in the spirit of minimal flavor violation [33], that decays to $\tau\tau$ dominate. These are also the least constrained because of the difficulty of τ identification, but the mass range $m_{\eta_{ST}} \sim 100 - 300$ GeV where the constraints have been reported for this channel is quite relevant for our models, ruling out $m_{\eta_{ST}} < 200$ GeV in this channel. If η_{ST} decays predominantly into ee or $\mu\mu$, the more stringent constraint $m_{\eta_{ST}} > 460$ GeV applies.

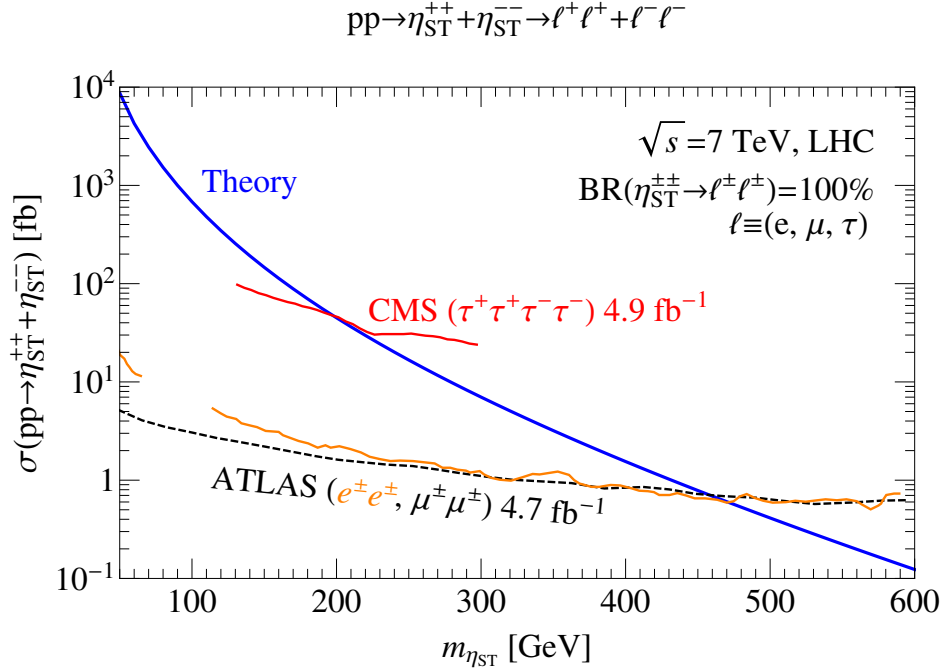


Figure 4. Constraints on the production cross section for pairs of η_{ST} mesons from same-sign dilepton searches of CMS [31] and ATLAS [32], and the prediction of the loop model. The mass range near m_Z yields no limits for the ee channel due to the large background from $Z \rightarrow e^+e^-$ with a charge misidentification.

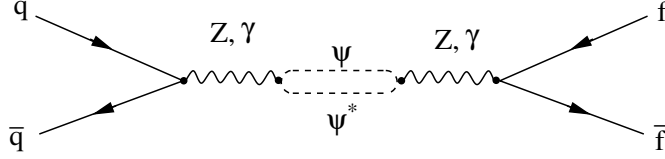


Figure 5. Process that gives opposite-sign dilepton peaks in the s-channel resonance. The bound state is a vector “meson” of the $SU(2)_d$ gauge sector, denoted by ϕ_ψ .

5 Vector “meson” production

If the pair SS^* or $\psi\bar{\psi}$ is produced with net angular momentum $J = 1$, it can form a single vector meson bound state analogous to the ϕ of QCD, rather than hadronizing into two mesons, as shown in fig. 5.³ We refer to such states as ϕ_s or ϕ_ψ in the models under consideration. Once produced, the ϕ can decay into leptons or quarks. Here we consider the decay into leptons since it provides a lower-background signal that has been searched for at the LHC. The process can be viewed as a mixing of ϕ with the virtual photon or Z boson,

$$q\bar{q} \rightarrow \gamma^*/Z \rightarrow \phi \rightarrow \gamma^*/Z \rightarrow e^+e^- \quad (5.1)$$

For center of mass energies much greater than m_Z , we can replace the intermediate γ and Z with the weak hypercharge gauge boson, allowing us to approximate $\Gamma(\phi \rightarrow \gamma^*/Z \rightarrow e^+e^-) = \Gamma(\phi \rightarrow \gamma^* \rightarrow e^+e^-)/\cos^2\theta_W$. The parton level production cross section is then

$$\sigma(q\bar{q} \rightarrow \phi \rightarrow e^+e^-) = \frac{4\pi q_q^2}{\cos^4(\theta_W)} \frac{\Gamma^2(\phi \rightarrow e^+e^-)}{(\hat{s} - m_\phi^2)^2 + m_\phi^2 \Gamma^2(\phi \rightarrow \text{any})} \quad (5.2)$$

where the Breit-Wigner form of the resonance is assumed; here the partial width refers to electromagnetic processes only, while the full width includes the contribution from the Z . The observed signal is proportional to the area under the resonance curve, which goes like $\Gamma(\phi \rightarrow e^+e^-)$ times the branching ratio for $\phi \rightarrow e^+e^-$.

In the case of fermionic constituents, ϕ_ψ is just like the ϕ of QCD, having orbital angular momentum $l = 0$ and getting its spin from that of the constituents. Then the decay width of ϕ_ψ to electrons is [34]

$$\Gamma(\phi_\psi \rightarrow e^+e^-) = \frac{4\pi N_c}{3} \frac{\alpha^2 q_\psi^2}{E_\psi^2} |\Psi(0)|^2 \quad (5.3)$$

where $\Psi(0)$ is the wave function at the origin, $E_\psi = (p^2 + m_\psi^2)^{1/2}$ is the kinetic energy of the constituent, and $q_\psi = 1/2$ in the MDM model. On the other hand, ϕ_s must have $l = 1$ and this leads to the different result (see appendix A)

$$\Gamma(\phi_s \rightarrow e^+e^-) = \frac{8\pi N_c}{3} \frac{\alpha^2 q_s^2}{E_s^2 m_\phi^2} |\vec{\nabla}\Psi(0)|^2 \quad (5.4)$$

To estimate the wave function factors, we appeal to a semiclassical model of mesons using a linear confining potential with tension k_d , outlined in appendix B. In the nonrelativistic case, the size of the meson is expected to scale as $(mk)^{-1/3}$ if m is the mass of the constituents, and therefore

³We take ϕ or J/ψ rather than Υ as the closer analogy because we are interested in the situation where the constituent masses are below the confinement scale, in order to avoid light glueballs, as discussed in section 2.4.

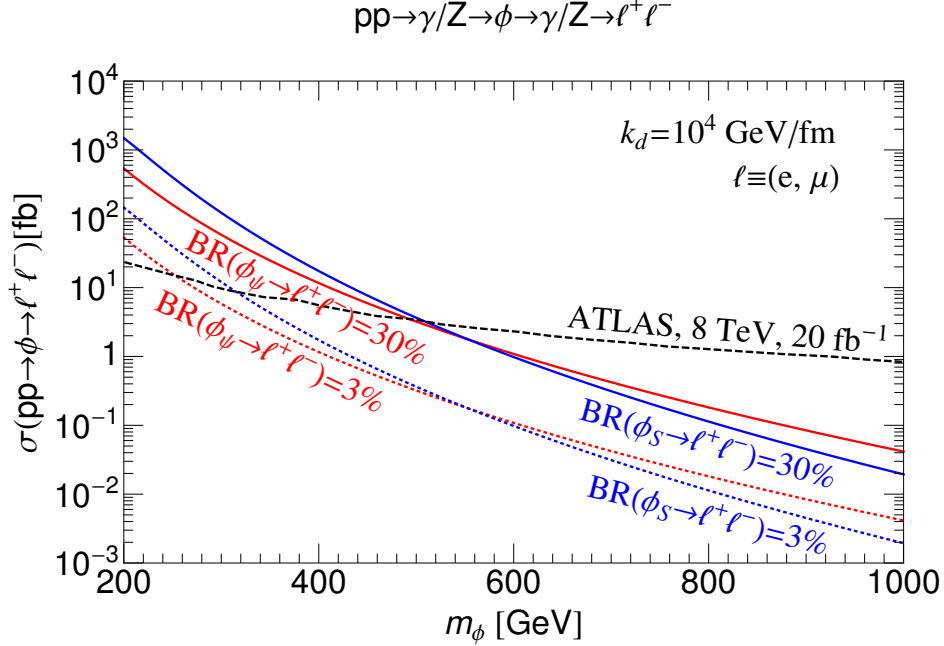


Figure 6. LHC constraints [35] on opposite sign same flavor dilepton resonances. We take 3% or 30% for the branching ratios into leptons $\ell^+ \ell^- = e^+ e^- + \mu^+ \mu^-$.

$|\Psi(0)|_{\phi_\psi}^2 \sim m_\psi k_d$ where k_d is the string tension of the $SU(N)_d$ interaction. Applying eq. (5.3) to the J/ψ of QCD, one obtains $|\Psi(0)|_{J/\psi}^2 = (0.6 \text{ fm})^{-3}$. Then we get the estimate

$$\frac{|\Psi(0)|_{\phi_\psi}^2}{|\Psi(0)|_{J/\psi}^2} \cong \frac{m_\psi k_d}{m_c k_{QCD}} \cong 10^6 \quad (5.5)$$

where we took $k_d/k_{QCD} = 10^4$, corresponding to a confinement scale of order 100 GeV, and $m_\psi/m_c = 100$ since the charm quark mass is ~ 1.3 GeV. To estimate $\vec{\nabla}\Psi(0)$ for the $\phi_S(1P)$ state, we take

$$|\vec{\nabla}\Psi(1P)| \sim |\vec{p}||\Psi(1S)| \quad (5.6)$$

where the momentum of the constituent is $p \sim (2\mu k_d)^{1/3} = (m_s k_d)^{1/3}$ for the $n = 2$ excited state ϕ_S . We will also consider the relativistic regime in which $k_d \gg m_s^2$. In that case the r.h.s. of (5.5) is replaced by $(k_d/k_{QCD})^{3/2}$, and the estimate for p in (5.6) becomes $p \sim (k)^{1/2}$. One can use a relativistic bound state from QCD instead of J/ψ for the comparison of (5.5) in that case; the ϕ of QCD is estimated to have $|\psi(0)|^2 = (1.6 \text{ fm})^{-3}$.⁴ To interpolate between the relativistic and nonrelativistic regimes, we fit the QCD wave functions to the ansatz $|\psi(0)|^2 = ak^{3/2} + bmk$, taking $a = 0.022$ and $b = 0.13$.

We applied LHC constraints on decays to $e^+ e^-$ plus $\mu^+ \mu^-$ final states to our models, following the recent ATLAS analysis [35] which utilized approximately 20 fb^{-1} integrated luminosity of data at 8 TeV center-of-mass energy, and also the recent CMS analysis [36] with the dielectron (dimuon) events sample corresponding to 19.6 (20.6) fb^{-1} integrated luminosity. Since the event samples from

⁴We correct the result given in [34] by taking into account the relativistic energy of the constituent rather than just its mass in eq. (5.3))

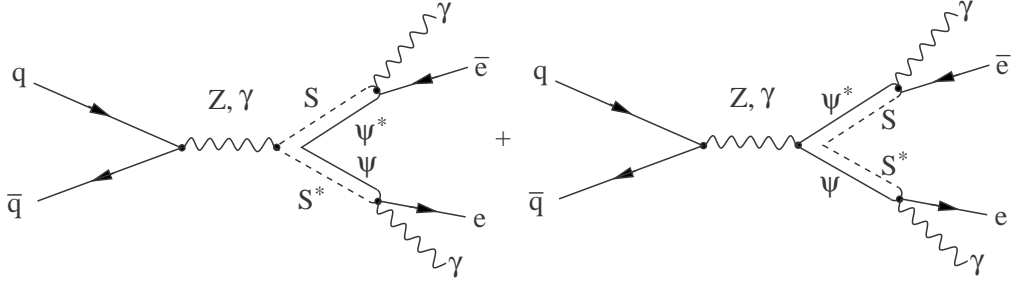


Figure 7. Feynman diagrams for production of N^\pm mesons that mimic excited electrons decaying to $e^\pm\gamma$.

both ATLAS and CMS are comparable in size and the limits on the sequential standard model Z' are also similar, we compare the vector meson production with only the expected 95% C.L. limits on $\sigma(\phi) \times \text{BR}(\phi \rightarrow \ell^+\ell^-)$ from the ATLAS analysis. Fig. 6 shows the theory predictions for these final states from the ϕ_S and ϕ_ψ resonances, assuming $q_S = 2$, $q_\psi = 1/2$, and leptonic branching ratios of 3% or 30%. The maximum possible branching ratio is determined by the available fermionic standard model states: $\text{BR} = 1/(3 + 1 + 8/3) = 0.15$ for a single lepton flavor. We will argue in section 9 that the true value in the loop or MDM models should be closer to 3% due to competing decay channels that are lower order in α .

From fig. 6 we infer the bounds $m_{\phi_S}, m_{\phi_\psi} > 500$ GeV if the branching ratio for ϕ decays into leptons is 30%. This limit goes down to 310 GeV and 250 GeV, respectively for m_{ϕ_S} and m_{ϕ_ψ} , when the branching ratio is 3%. In sect. 9 we will argue that these limits are not difficult to satisfy in the dark matter models since we have the freedom to make the confinement scale of the $\text{SU}(N)_d$ interactions sufficiently large.

6 Excited electron/muon limits

In the MDM model, there are four possible hadronization processes that the scalar particle S can undergo to form different bound states after being pair-produced.⁵ One of these results in pairs of charged particles $N^- = S^*\psi$ and $N^+ = S\bar{\psi}$ with the same quantum numbers as the right-handed electron and positron. N^- in fact mixes with e_R and higher generation leptons through the Yukawa interaction $y_i\epsilon_{ab}S_a^*\bar{l}_{R,i}\psi_b$, where i is the generation index. In the low-energy theory below the confinement scale, this operator induces off-diagonal mass terms $m_i\bar{l}_{R,i}N^-$, where $m_i = y_i\langle 0|\epsilon_{ab}S_a^*\psi_b|N^-\rangle$. Couplings such as $\bar{N}Ae$ which were absent in the original flavor basis are not induced by diagonalizing the mass matrix. However, since N^- has a magnetic moment that is much smaller than that of the leptons (ψ being heavy), a transition magnetic moment is induced between the leptonic and exotic mass eigenstates. Thus the decay $N^- \rightarrow e + \gamma$ can occur, which mimics the excited electron search signals predicted for example by extra-dimensional models with Kaluza-Klein excitations of the electron. The production and decay process is illustrated in fig. 7.

We have estimated the production cross section for N^+N^- pairs leading to $l^\pm\gamma$ final states at the LHC in the MDM model. In the first approximation, it is the same as that for producing the unhadronized $\psi\bar{\psi}$ pair, whose cross section is 4 times greater than that for producing SS^* at high energies. Taking into account hadronization is expected to reduce this estimate by a factor of ~ 4 since

⁵Because we have assumed the gauge group is $\text{SU}(2)_d$, S can bind with any of S , S^* , ψ or $\bar{\psi}$.

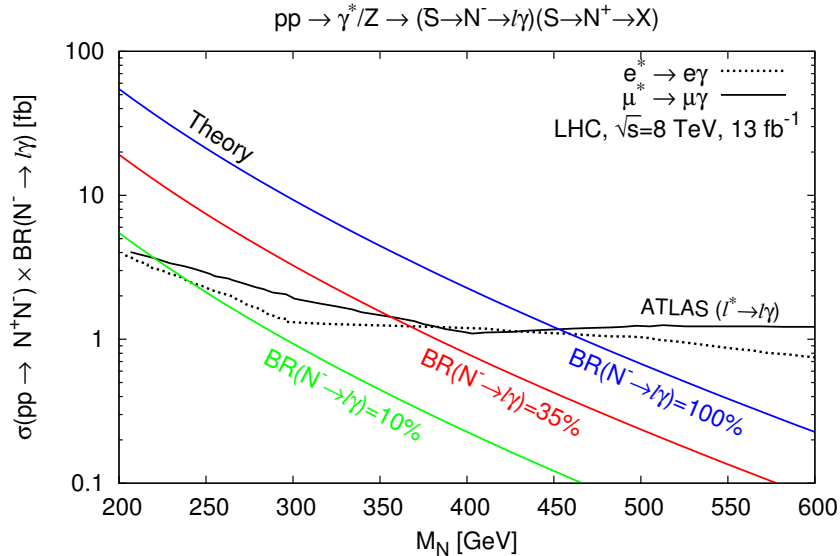


Figure 8. Limits resulting from excited electron and muon searches, and predictions of the MDM model assuming that the branching ratio for the charged bound state decay $N^- \rightarrow \ell^- \gamma$ is 10%, 35% and 100%, respectively.

there are four possible color-neutral final states involving ψ ($\psi\psi$, $\psi\bar{\psi}$, ψS and ψS^*). The predictions are shown in fig. 8 for several representative values of the branching ratio for $N^- \rightarrow \ell^- \gamma$, where l stands for e or μ . Upper limits on this cross section have been derived by looking for peaks in the distribution of the invariant mass of the electron and the photon. ATLAS has searched $\sim 13 \text{ fb}^{-1}$ data at 8 TeV for this final state [37]. The resulting constraint for electrons is $\sigma(e^*) \times \text{BR}(e^* \rightarrow e\gamma) < (0.6 - 1) \text{ fb}$ when $m_{N^\pm} > 400 \text{ GeV}$, and for muons $\sigma(\mu^*) \times \text{BR}(\mu^* \rightarrow \mu\gamma) < (0.7 - 1) \text{ fb}$ when $m_{N^\pm} > 400 \text{ GeV}$. We will discuss the impact on the MDM model of 130 GeV dark matter in section 9.2.

7 Two- and four-photon events

One of the striking signatures in our models is the 4-photon event arising from decays of meson pairs, either $2\eta_s$ or $2\eta_\psi$. Fig. 9(a) shows the production process for $pp \rightarrow 2\eta_s$ followed by $\eta_s \rightarrow 2\gamma$ for each η_s . The branching ratio into photons is significant as long as there are no lighter hadrons of the $\text{SU}(N)_d$ interaction, notably glueballs, and if decays into dark matter do not dominate. The first assumption was previously made in order to forbid glueballs as annihilation products of dark matter, which would strongly suppress its relic density. The second one is model-dependent, as we will discuss in section 9. The 4-photon final state is a very clean channel because the primary standard model background is from analogous QCD processes in which π^0 and η mesons are produced; these photon pairs will not have peaks in their invariant mass spectra except at very low values, and are unlikely to pass the photon identification criteria at LHC discussed in more detail later. There is also a perturbative contribution to $q\bar{q} \rightarrow 4\gamma$ from fig. 9(b), but this is smaller by $O(\alpha^2)$, along with other small backgrounds that we discuss below. The four-photon signal has not yet been searched for by ATLAS or CMS so we do not yet obtain any constraints from having two pairs of photons. Instead,

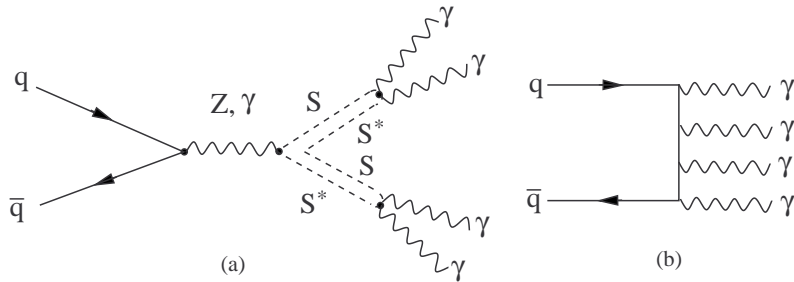


Figure 9. (a) (left) Four-photon event from production of η_S pair followed by $\eta_S \rightarrow \gamma\gamma$. (b) (right) Higher order standard model background process for four-photon events.

we make a preliminary study of this channel in section 7.2. However the four-photon channel will also contribute to existing searches for single photon pairs and we can use these to set limits, which we present in section 7.1.

7.1 Diphoton constraints

Diphotons would be observed from the process shown in fig. 9(a) since existing searches do not discriminate against events producing more than two photons. Here we approximate the η_S meson pair production cross section as half that of the elementary SS^* pair in the loop model, since there are two ways to hadronize into mesons, whereas in the MDM model we take production of η_ψ pairs to be equal to 1/4 that of $\psi\bar{\psi}$ since there are four possible final states. We estimate the diphoton production cross section as

$$\sigma(\gamma\gamma) = 2 \sigma(pp \rightarrow \eta\eta) \text{BR}(\eta \rightarrow \gamma\gamma) \quad (7.1)$$

where $\text{BR}(\eta \rightarrow \gamma\gamma)$ is the diphoton branching ratio of η decays and the factor of 2 accounts for the two pairs of photons that reconstruct to the right invariant mass. In the loop model this may overestimate the production since we ignore “baryonic” final states, SSS , SST and STT .

Both ATLAS and CMS have provided limits on the diphoton production cross sections using LHC data at energy $\sqrt{s} = 7$ TeV with integrated luminosity $\mathcal{L} = 4.9 \text{ fb}^{-1}$ (ATLAS) [38] and $\mathcal{L} = 2.2 \text{ fb}^{-1}$ (CMS) [39]. Here we apply the ATLAS limits to our models. Fig. 10 shows the ATLAS constraints on the diphoton final states in the mass range > 409 GeV. The diphoton limits in the low mass range 122–409 GeV are estimated based on the number of events observed by ATLAS. The theory predictions of the diphoton signals from η_S or η_ψ meson decay are also plotted assuming $\text{BR}(\eta \rightarrow \gamma\gamma) = 100\%$. Comparison indicates that meson masses $m_{\eta_\psi} < 120$ GeV and $m_{\eta_S} < 200$ GeV are excluded with the integrated luminosity 4.9 fb^{-1} . We note that the diphoton analyses for the SM Higgs boson search near 120 GeV of ATLAS [40] and CMS [41] were both based on the integrated luminosity $\sim 25 \text{ fb}^{-1}$. A dedicated analysis from these larger data sets would further improve the limit on m_{η_ψ} .

7.2 4-photon final state

To simulate the LHC signals of the 4-photon events, we computed the matrix elements of the production processes using MadGraph4 [42], taking an effective field theory approach to model the couplings to two photons. We assumed the nonrenormalizable interaction

$$\mathcal{L} = g\eta_S F^{\mu\nu} F_{\mu\nu} \quad (7.2)$$

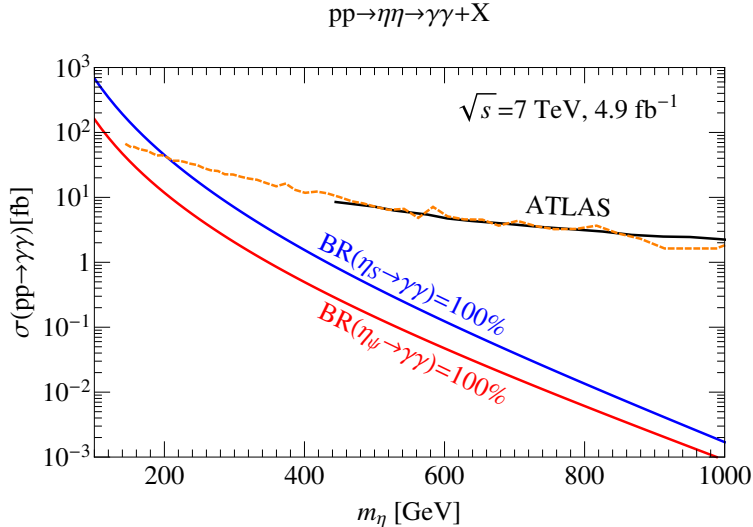


Figure 10. Constraints on the diphoton production cross section from the ATLAS analysis [38]. The solid (dashed) ATLAS curves correspond to the actual (approximated) 95% C.L. limits in the diphoton channel. The dashed ATLAS curve which extends the limits to the low mass range (control region in the ATLAS analysis) is estimated using $\sigma < 2\sqrt{N_{\text{SM}}}/(\mathcal{L} \times A)$, where N_{SM} is the standard model prediction, $\mathcal{L} = 4.9 \text{ fb}^{-1}$ is the integrated luminosity, and the assumed acceptance is chosen to be $A \sim 25\%$ such that the estimated limits agree with the actual limits in the high mass region. The production cross sections from η_S and η_ψ meson decays are also plotted assuming 100% branching ratio to diphotons.

where the coupling strength, g , has the dimensionality of inverse mass.

We computed the parton level cross sections both for the dark matter models using the effective theory approach and for the standard model in MadGraph. The results were then transmitted to PYTHIA [43] for hadronization and PGS [44] for collider simulations. Following the ATLAS analysis [38], we select only the photon candidates with transverse momentum $p_T > 25 \text{ GeV}$, and the pseudorapidity in the ranges $|\eta| < 1.37$ or $1.52 < |\eta| < 2.37$ (to benefit from the high granularity of the first layer in the electromagnetic calorimeter for discriminating between genuine prompt photons and faked photons within jets) [45]. An isolation requirement on the photon is further imposed: the photon in the vicinity of a jet with $p_T > 10 \text{ GeV}$ is vetoed if the angular distance between the photon and the jet, $\Delta R = \sqrt{\Delta\eta^2 + \Delta\phi^2}$, is less than 0.4. After these selection cuts, only the events that contain 4 photons are considered. We then search for the correct pairings of photons, by demanding that they lead to the smallest difference between the two invariant masses out of the 3 possible combinations. The resulting invariant mass distribution for the case where $m_{\eta_S} = 300 \text{ GeV}$ and $\Gamma_{\eta_S} = 1 \text{ GeV}$ is given in Fig. 11(a) as an example of the kind of signal that could be expected. We then compare the signal events that have both invariant masses within a fixed 20 GeV mass bin to the standard model events satisfying the same selection criteria to derive the discovery limits for this final state. The efficiency of this selection for the signal events is estimated to be 50% based on the sample study shown in Fig. 11(a).

In sect. 7.1 we determined the maximum cross section for diphoton production allowed for the models. These imply 4-photon cross sections of 70 fb from η_ψ pairs at $m_{\eta_\psi} = 120 \text{ GeV}$, and 21 fb from η_S pairs at $m_{\eta_S} = 200 \text{ GeV}$. Thus we would predict about 170 and 50 four-photon events respectively

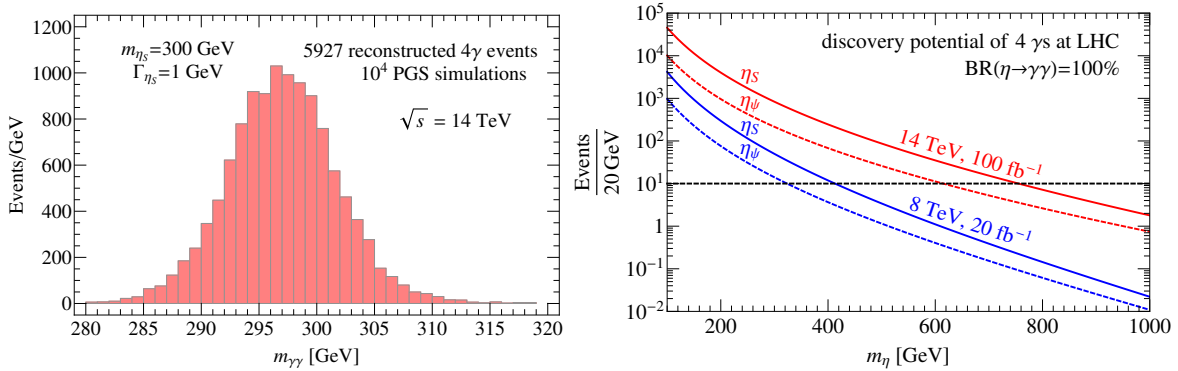


Figure 11. (a) (left) Reconstruction of the 4-photon events from PGS simulation. The pairing of photon that results in least mass difference is chosen for the invariant mass distribution. The shape of the distribution is broadened by the energy resolution of the detector. (b) (right) Solid (dashed) lines are the predicted number of 4-photon events per 20 GeV invariant mass bin, from $\eta_s \rightarrow \gamma\gamma$ ($\eta_\psi \rightarrow \gamma\gamma$) for $\sqrt{s} = 14$ TeV, $\int \mathcal{L} dt = 100$ fb $^{-1}$ (upper pair of curves), and for $\sqrt{s} = 8$ TeV, $\int \mathcal{L} dt = 20$ fb $^{-1}$ (lower pair of curves). Horizontal line shows the discovery criterion of 10 events for reference.

in these two models, for the 4.9 fb $^{-1}$ data set, suggesting that a dedicated four-photon search could improve the limits. We have simulated these events and the background in greater detail in order to forecast the improvement in constraints, or potential for discovery, from searching for this signal. The result is shown in fig. 11(b). We simulated the SM background shown in fig. 9(b) which gives rise to a cross section of only 0.1 – 0.2 fb for $\sqrt{s} = 8 - 14$ TeV and $p_T(\text{photon}) > 10$ GeV in the MadGraph5 [46] simulation. Our simulation further shows that only about 2% of these SM 4-photon events can pass the selection cuts and the invariant mass requirement, which then contributes about only 0.4 events for the case where $\sqrt{s} = 14$ TeV and $\mathcal{L} = 100$ fb $^{-1}$ at the LHC.

To check the SM backgrounds due to contamination from QCD and electron misidentification, we further compute the parton level cross sections in MadGraph for various SM processes shown in Table. 1. To estimate the faked photons originating from hadronic jets and isolated electrons, we use the fake rates (or background rejection) analyzed by the ATLAS collaboration. The jet backgrounds can be reduced by a factor of ~ 5000 using the tight photon selection in ATLAS, with an additional improvement by a factor of ~ 1.5 by adding isolation requirements [47]. The rejection for quark-initiated and gluon-initiated jets with $E_T > 20$ GeV are about 1.6×10^3 and 1.4×10^4 respectively [47]. Here we assume a conservative jet rejection based on the quark-initiated jets, $R \sim 2 \times 10^3$, and thus obtain the fake rate $\sim 5 \times 10^{-4}$ (the inverses of the rejection). For the faked photons due to misidentified electrons, we use the measured faked rate $f_{\gamma \rightarrow e} = 0.062$ [48]. The effective 4-photon production cross sections are then computed taking into account the faked rates for various SM processes. As shown in Table. 1, the 4-photon events at LHC due to contamination are generally smaller than the $\gamma\gamma\gamma\gamma$ process shown in fig. 9(b), and only $\gamma\gamma\gamma j$ and $\gamma\gamma ee$ processes can yield sizable contributions comparable to the $\gamma\gamma\gamma\gamma$ process. We further simulated the $\gamma\gamma\gamma j$ and $\gamma\gamma ee$ processes in PYTHIA and PGS for the case $\sqrt{s} = 14$ TeV and $\mathcal{L} = 100$ fb $^{-1}$, but no event with invariant mass pair above 100 GeV was found from these two SM processes.

Since the SM background is thus shown to be very small, we ignore its contribution, and take

SM process	$\gamma\gamma\gamma\gamma$	$\gamma\gamma\gamma j$	$\gamma\gamma jj$	γjjj	$jjjj$	$\gamma\gamma\gamma e\nu$	$\gamma\gamma ee$	$\gamma eee\nu$	$eeee$
σ_{parton} [pb]	$2\cdot 10^{-4}$	$2\cdot 10^{-1}$	$1\cdot 10^2$	$3\cdot 10^4$	$2\cdot 10^7$	$6\cdot 10^{-5}$	$5\cdot 10^{-2}$	$9\cdot 10^{-4}$	$7\cdot 10^{-3}$
$\sigma_{4\gamma}$ [pb]	$2\cdot 10^{-4}$	$1\cdot 10^{-4}$	$3\cdot 10^{-5}$	$4\cdot 10^{-6}$	$1\cdot 10^{-6}$	$4\cdot 10^{-6}$	$2\cdot 10^{-4}$	$2\cdot 10^{-7}$	$1\cdot 10^{-7}$

Table 1. The parton level cross section and the estimated cross section for the 4-photon final states for various SM processes at the LHC with $\sqrt{s} = 14$ TeV. The faked rates 5×10^{-4} (0.062) for photons originating from jets (electrons) are assumed here for the estimation of the 4-photon cross sections. The parton level cross sections are computed with the transverse momentum cuts: $p_T(\text{jet}) > 20$ GeV, $p_T(\text{photon}) > 10$ GeV, $p_T(\text{lepton}) > 10$ GeV in MadGraph.

$N = 10$ events as the criterion for discovery of 4-photons in these models. The Fig. 11(b) indicates that the reach for discovering the hidden meson states at LHC is up to 400 GeV for η_S at $\sqrt{s} = 8$ TeV with the integrated luminosity already collected, and up to 750 GeV at $\sqrt{s} = 14$ TeV with 100 fb^{-1} integrated luminosity. The corresponding mass values are somewhat smaller for the η_ψ due to the smaller electric charge of ψ .

8 Monophoton limits

One way in which constraints on vector mesons (section 5) could be evaded is if the branching ratio for ϕ decays into leptons is small due to more dominant decays into dark matter or other final states. In this case, a complementary constraint can be obtained from searching for monophoton events such as those depicted in fig. 12. In generic dark matter models, the monophoton arises as initial state radiation (ISR) from the quarks, but for the loop model that we consider, the vector meson ϕ_S cannot decay only into dark matter particles, because in this model the DM is scalar and $\chi\chi$ cannot have the J^{PC} quantum numbers to match those of ϕ_S . However there is a decay channel $\phi_S \rightarrow \gamma\eta_S$ or $\phi_S \rightarrow \gamma\eta_T$ followed by $\eta_{S,T} \rightarrow \chi\chi$, as shown in fig. 12(a), that produces a monophoton and missing energy. It can naturally dominate over the leptonic decays $\phi_S \rightarrow \ell^+\ell^-$ since it is lower order in α . It is mediated by the effective operator

$$g_{S,T} \frac{eq_S}{m_\phi} \phi_S^{\mu\nu} F_{\mu\nu} \eta_{S,T} \quad (8.1)$$

where we estimate $g_S = 1.5$ by using the same interaction to model the charmonium radiative decay processes, $\chi_{c0} \rightarrow \gamma J/\psi$, $J/\psi \rightarrow \gamma\eta_c$, and $\psi(2S) \rightarrow \gamma\chi_{c0}$. We estimate the ratio $g_T/g_S \simeq \alpha_d^2/\pi$, which encodes the OZI suppression due to the extra gluon loop for η_T final states, by comparing the radiative

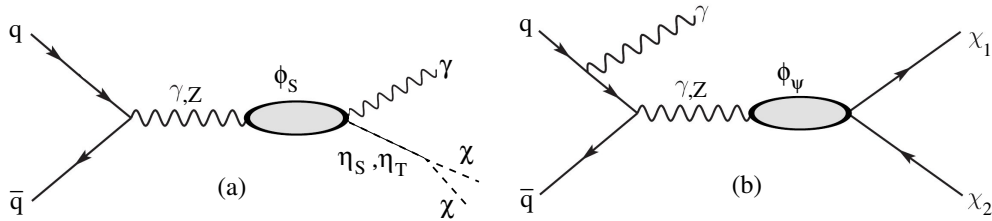


Figure 12. Feynman diagrams that generate the monophoton signal for (a) loop model; (b) MDM model.

decays $J/\psi \rightarrow \gamma\eta_c$ and $J/\psi \rightarrow \gamma\eta'$ in QCD in the same model. Here $\alpha_d = g_d^2/4\pi$ is the strength of the $SU(N)_d$ gauge interaction, evaluated at the scale m_η [49]. We take the coupling to run according to the one-loop beta function,

$$\alpha_d(Q^2) = \frac{12\pi}{32 \ln(Q^2/\Lambda_d^2)} \quad (8.2)$$

calculated for $SU(3)$ at scales where T is the only light fundamental matter. By comparing to the running of the QCD coupling, we infer that $\Lambda_d \cong k_d^{1/2}/2$ in the log.

In contrast, monophotons in the MDM model arise from initial state radiation, but in this case the DM particles produced by decay of the vector meson ϕ_ψ cannot be identical. This is because the decay is mediated by the effective interaction $\phi_\psi^\mu \bar{\chi}_1 \gamma_\mu \chi_2$ that couples ϕ_ψ to the DM ground state χ_1 and the first excited state χ_2 (there are three Majorana DM states in this model, of which only the least massive one is stable). The decay to $\chi_1\chi_1$ is forbidden since the vector current $\bar{\chi}_1 \gamma_\mu \chi_1$ vanishes identically for Majorana particles. The process is depicted in fig. 12(b). Searches for LHC events with a single energetic photon (or jet) plus a large missing momentum have been frequently used to constrain the interaction strength of dark matter with standard model fermions [50–52]. The signature is a high p_T photon event accompanied by a significant amount of missing energy.

In the models we consider, the main parameters controlling the cross section for monophoton events are the mass m_ϕ of the $\phi_{s,\psi}$ mesons and their coupling to the photon or Z boson, as well as the mass of $\eta_{s,T}$ in the loop model, or $\chi_{1,2}$ in the MDM model. In sect. 5 we showed that the coupling of the vector boson to photons was proportional to the wave function of the origin (for ϕ_ψ) or its gradient (for ϕ_s). These in turn depend upon the string tension k_d of the $SU(N)_d$ gauge interaction through eqs. (5.5, 5.6). For low values of k_d , such that $k_d < m_{\psi,s}^2$, k_d and m_ϕ can be treated as independent parameters, while for $k_d \gg m_{\psi,s}$, we expect that $m_\phi \sim k_d^{1/2}$, as outlined in appendix B. The masses of the final state particles χ_2 or $\eta_{s,T}$ are also determined by k_d when it becomes large compared to $m_{\psi,s}$. We expect that m_{ϕ_s} is some multiple of m_{η_s} , roughly independent of k_d , while for moderate values of k_d , the η_T can be kept relatively light since m_T may be significantly less than m_s . In the MDM model, χ_2 , which is mostly a bound state of $S\bar{\psi}$, is expected to have $m_{\chi_2} \sim m_{\eta_\psi}$ for large k_d . In sect. 9.2 we will show that it is possible to make m_{χ_1} parametrically smaller than $k_d^{1/2}$ even when k_d is large.

To determine the LHC constraints from monophotons, we first computed the parton level cross sections for the processes shown in fig. 12 using MadGraph. The detector acceptance and efficiency were determined using PYTHIA and PGS simulations. Following the ATLAS analysis [52], a minimum photon p_T of 80 GeV was required for the event simulations with MadGraph. For the events simulated with PYTHIA and PGS, we imposed the following sets of selection cuts: (1) events were required to have $E_T^{\text{miss}} > 150$ GeV; (2) a photon was required with $p_T > 150$ GeV and $|\eta| < 1.37$ or $1.52 < |\eta| < 2.37$; (3) events with more than one jet with $p_T > 30$ GeV and $|\eta| < 4.5$ were rejected; (4) events with identified electrons (muons) with $p_T > 20$ GeV and $|\eta| < 2.47$ ($p_T > 10$ GeV and $|\eta| < 2.4$) were rejected; (5) The angular separations between the photon, the missing transverse energy, and the jet, $\Delta\phi(\gamma, E_T^{\text{miss}})$, $\Delta R(\gamma, \text{jet})$, $\Delta\phi(\text{jet}, E_T^{\text{miss}})$, were all required to be larger than 0.4. For the MDM model with the vector meson mass in the range 200–1000 GeV, the detector efficiency for our simulations is found to be $A \times \epsilon \sim (14\%–27\%)$, which is in the same range as the detector efficiencies for the various DM effective operator interactions in the ATLAS analysis [52].

The LHC production cross section for monophoton final states taking into account the detector effects was then computed for the case where the vector meson decays into hidden sector fermion pairs (MDM model), or into a single photon plus two dark matter particles (loop model). In the loop model,

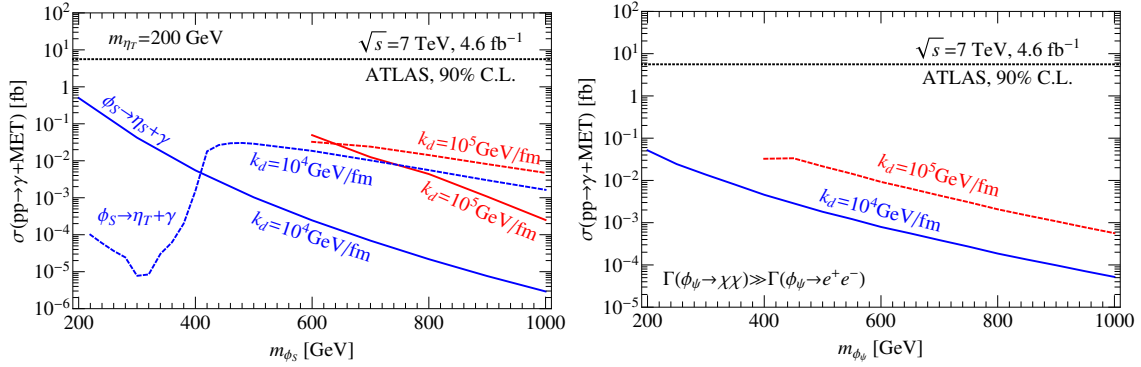


Figure 13. (a) (left) Upper line (dotted): ATLAS constraint on the cross section for monophoton production. Dashed curves: predictions of loop model for $\phi_S \rightarrow \eta_T + \gamma$ at the values $k_d = 10^4, 10^5$ GeV/fm of the $SU(N)_d$ string tension. Solid curves: similar to dashed but for $\phi_S \rightarrow \eta_S + \gamma$. (b) (right) analogous monophoton constraints from ISR in the MDM model, at $k_d = 10^4, 10^5$ GeV/fm.

we computed the branching ratios of the ϕ_S decaying into $\gamma\eta_S$ and $\gamma\eta_T$, and found that these dominate over the decays into SM final states. In the MDM model, we assume that the invisible decays of the ϕ_S dominate. As shown in fig. 13, we find that the monophoton constraint is more stringent for the loop model than for the MDM model. This is partly because the cross section for the latter process is down by $O(\alpha)$, since the photon comes from the initial state, whereas it arises from the decay of ϕ_S in the former. This statement is true however only if the final state photon is energetic enough to pass the imposed cut, $E_\gamma > 150$ GeV. Based upon the “Bohr model” predictions of appendix B, we find that this is not the case for $\phi_S \rightarrow \eta_S + \gamma$, whereas it is true for $\phi_S \rightarrow \eta_T + \gamma$ at sufficiently high $m_{\phi_S} \gtrsim 350$ GeV, if we assume that m_{η_T} is fixed to be 200 GeV. This explains the qualitative behavior of the $\phi_S \rightarrow \eta_T + \gamma$ curve for $k_d = 10^4$ GeV/fm in fig. 13(a). None of these predicted cross sections conflicts with the ATLAS upper limit.

The monophoton signals arising from the MDM model with the string tension in the range $10^4 - 10^5$ GeV/fm are also significantly below the ATLAS 90% C.L. limit, 5.6 fb, as shown in fig.13(b). For higher k_d , for example 10^6 GeV, the mass of ϕ_S exceeds 1 TeV and so the resulting prediction would not appear in the range of masses plotted (and moreover would still be below the upper limit). Thus the MDM model is not constrained by the current monophoton searches.

9 Viability of 130 GeV (and other) DM models

In this section we combine the preceding LHC constraints with the requirements from sect. 2 of the Fermi 130 GeV line to determine what regions of parameter space of the models under consideration are compatible with all the data. After considering the three classes of models, we sketch how the most relevant of these results would generalize to potential dark matter candidates of other masses, resulting in gamma ray lines at different energies.

9.1 Loop model

In order to get a large enough cross section for $\chi\chi \rightarrow \gamma\gamma$, eq. (2.2) implies that m_S must not be too much larger than m_χ , so that the loop is resonantly enhanced; otherwise nonperturbatively large

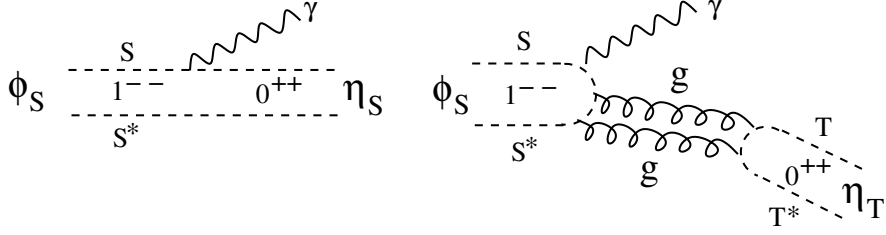


Figure 14. Dominant decays of ϕ_S vector meson, which reduce the branching ratio for leptonic final states. The second process, where g stands for the $SU(N)_d$ gluons, exists only in the loop model, while the first is present in both models.

values of the coupling $\lambda_{S\chi}$ are required. To make the r.h.s. of (2.2) equal to 1 for the fiducial values of parameters given there, one finds that $m_S = 147$ GeV. Smaller values of $m_S > 130$ GeV would allow for $\lambda_{S\chi} < 3$, with a minimum value of $\lambda_{S\chi} = 1$ when m_S is just above 130 GeV. Thus the range of allowed values is limited to $m_S \sim 130 - 147$ GeV.

The constraint from same-sign dileptons, fig. 4, can be evaded if the branching ratio of η_{ST} into ee or $\mu\mu$ is sufficiently small, or if $m_{\eta_{ST}} > 200$ GeV in the case of 100% branching to $\tau\tau$. The models we consider do not specify the relative couplings of η_{ST} into different flavors of leptons, but if we adopt some version of minimal flavor violation, it would be natural to expect that the partial widths for ee , $\mu\mu$ and $\tau\tau$ final states are in the ratio $m_e^2 : m_\mu^2 : m_\tau^2$. Thus we require that $m_{\eta_{ST}} > 200$ GeV. Since $m_S > 130$ GeV, this will be satisfied if $m_T > 70$ GeV, and perhaps for smaller values, depending upon how much of $m_{\eta_{ST}}$ is due to the gluons of $SU(N)_d$.

Direct production of the vector meson ϕ_S followed by its decay into leptons is potentially constraining, but this depends upon the branching ratio of ϕ_S into leptons (and into quarks, because of the production part of the amplitude). In fact, there are more dominant decay channels $\phi_S(1P) \rightarrow \eta_S(1S) + \gamma$ and $\phi_S(1P) \rightarrow \eta_T(1S) + \gamma$ shown in fig. 14. These are lower order in the electromagnetic coupling than $\phi_S \rightarrow \ell^+\ell^-$ and are therefore expected to have a larger branching ratio by of order $1/\alpha$. The diagram with gluons is not suppressed (by the Okubo-Zweig-Iizuka (OZI) rule) in the case where the constituent masses are at the confinement scale. Taking 0.03 as a representative value of the leptonic branching ratio,⁶ we infer from fig. 6 the lower limit $m_{\phi_S} \gtrsim 310$ GeV, which requires $\phi_S(1P)$ to get $\gtrsim 5 - 15\%$ of its mass from the strong interactions as opposed to the constituent masses m_S . The meson mass is given by $m_\phi \cong 2m_S \lesssim 300$ GeV only if $m_S^2 \gg k_d$ (the string tension of $SU(N)_d$), but we have already argued that this regime is not allowed since otherwise dark matter would annihilate too strongly into glueballs of $SU(N)_d$. In the opposite limit $m_S^2 \ll k_d$, the meson mass scales as $\sqrt{k_d}$ (appendix B). Thus only a modest hierarchy in k_d/m_S^2 is needed to satisfy the dilepton constraint. If k_d/m_S^2 is not too large, this constraint would be close to saturation, hence leading to discoverable new physics.

The diphoton searches provide a weaker limit $m_{\eta_S} > 220$ GeV (fig. 10), which is automatically satisfied due to the constraint $m_S > 130$ GeV. It might be possible to improve this limit by doing a dedicated search for 4-photon events as we have suggested in sect. 7.2. However, the strength of these constraints depends upon the branching ratio for $\eta_S \rightarrow \gamma\gamma$. In this model, the invisible decays to dark

⁶ This number is motivated by the example $\Gamma(\phi \rightarrow e^+e^-)/\Gamma(\phi \rightarrow \eta\gamma) = 3 \times 10^{-2}$ from QCD

matter, $\eta_S \rightarrow \chi\chi$, are guaranteed to dominate since

$$\frac{\Gamma(\eta_S \rightarrow \gamma\gamma)}{\Gamma(\eta_S \rightarrow \chi\chi)} \cong \frac{\sigma(SS \rightarrow \gamma\gamma)}{\sigma(SS \rightarrow \chi\chi)} \sim \frac{(2e)^4}{\lambda_{S\chi}^2} \sim \frac{0.13}{9} \quad (9.1)$$

Recall that the coupling $\lambda_{S\chi}$ had to be rather large in order to get the observed galactic gamma ray line strength.

9.2 MDM Model

From eq. (2.4) one finds that the composite magnetic dark matter model requires the mass of the fermionic constituent to be $m_\psi \sim 70$ GeV in order to get a large enough magnetic moment to match the galactic observations. While this sounds dangerously low, the model has the interesting possibility of allowing for the confinement scale Λ_d to be parametrically higher than the DM ground state $m_{\chi_1} = 130$ GeV, because χ_1 is a mixed state of an elementary Majorana fermion χ (neutral under the $SU(2)_d$) and the Dirac bound state $\eta = S\psi$. The mixing is provided by the Yukawa interaction $y\bar{\chi}S\psi$ in the fundamental Lagrangian, leading to an off-diagonal mass term $m_y\bar{\chi}\eta$ in the low-energy effective theory, with $m_y \sim y\Lambda_d$. Considering for illustration the case where $m_\eta = m_\chi$ (m_χ being the mass of the original unmixed χ field), corresponding to maximal mixing, one has

$$m_{\chi_1} = m_\eta - \sqrt{2}m_y \quad (9.2)$$

(see eq. (C1) of ref. [25]). Thus if $m_\eta \sim \Lambda_d$ happens to be close to $\sqrt{2}m_y$, there can be a moderate hierarchy in Λ_d/m_ψ without excessive fine-tuning. This freedom can help the model to satisfy the LHC constraints, since then ψ only appears in bound states that are significantly heavier than its rather low bare mass.

First we consider the direct production of the vector meson ϕ_ψ followed by decays into leptons. In addition to the fermionic decay channels, there is a lower-order decay process $\phi_\psi(1S) \rightarrow \eta_\psi(1S) + \gamma$, similar to fig. 14, except now the final hadron has 0^{-+} quantum numbers. Therefore the $\eta_\psi(1S)$ and γ must be in an $l = 1$ state to conserve parity. This could in principle suppress the rate, since the effective interaction requires an extra derivative, but if the mass splitting between η_ψ and ϕ_ψ is of order the confinement scale, as would be the case assuming the moderate hierarchy between Λ_d and m_ψ mentioned above, there is no significant suppression. The analogous situation is observed in QCD for the decays of the $\bar{s}s$ vector meson ϕ ; see footnote 6. Taking 0.03 as the leptonic branching ratio gives the constraint $m_{\phi_\psi} \gtrsim 250$ GeV. In view of the preceding discussion, by taking $\Lambda_d \sim 300$ GeV, it would not be difficult to satisfy this constraint while keeping the lightest DM state at 130 GeV.

Next we turn to the limits from excited lepton searches. As mentioned in section 6, there is a transition magnetic moment between the charged bound states $N^- = S^*\psi$ and the right-handed leptons in the mass eigenstate basis. The mass mixing arises from the Yukawa interaction $y_\ell \epsilon_{ab} S_a^* \bar{\ell}_R \psi_b$ which in the low-energy theory can be represented by a mass term $y_\ell f_N \bar{\ell}_R N_L^-$, where $\langle 0 | \epsilon_{ab} S_a^* \psi_b | N^- \rangle = f_N$. For simplicity consider the case where only a single generation of leptons mixes significantly with N^- . For small y_ℓ , the mixing angle is $\theta \cong y_\ell f_N / m_N \sim y_\ell$, since by analogy with pions we expect $f_N / m_N \sim 1$. The transition magnetic moment is given by $\mu = \theta(\mu_\ell - \mu_N) \cong \theta\mu_\ell$, since we expect that $\mu_\ell \gg \mu_N$ due to the fact that $m_\ell \ll m_N$. The partial width for $N^- \rightarrow \ell^- \gamma$ is thus of order

$$\Gamma(N^- \rightarrow \ell^- \gamma) \sim \frac{y_\ell^2 \mu_\ell^2}{8\pi} m_N^3$$

Interestingly, if we make the assumption of minimal flavor violation so that $y_\ell \sim m_\ell$, the flavor dependence cancels out since $\mu_\ell \sim e/m_\ell$. In this case the branching ratio is roughly equal to all lepton

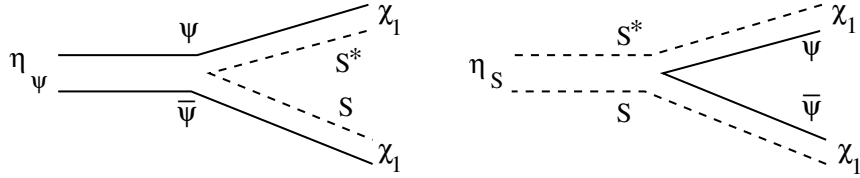


Figure 15. Dominant decays of η_ψ and η_S mesons into dark matter in the MDM model, which reduce the branching ratio for diphoton final states. The dark matter ground state χ_1 is actually an admixture of the ψS^* or $\bar{\psi} S$ bound state and a neutral Majorana fermion χ .

flavors. The search for excited electron decays (fig. 7) then gives the limit $m_N > 367$ GeV, which is somewhat stronger than the dilepton constraint. Nevertheless it can be accommodated by taking the confinement scale to be of this order.

The diphoton constraint from fig. 10, $m_{\eta_\psi} > 140$ GeV, is relatively weak, but as in the case of the loop model, it might be leveraged into a more sensitive test if 4-photon events were analyzed in the data. Again, this depends on the branching ratio for $\eta_\psi \rightarrow \gamma\gamma$. Like in the loop model, there exist more dominant decays of η_ψ (or η_S) into two dark matter particles. At the parton level, this is mediated by the diagrams in fig. 15, which are strong decays and not suppressed by any small couplings, but only by the mixing angle between the $\bar{\psi} S$ bound state and the χ_1 mass eigenstate (recall that χ_1 is an admixture of $\bar{\psi} S$ and a neutral Majorana fermion χ). This mixing angle is typically large, $\pi/4$ in the maximal mixing case exemplified in eq. (9.2). Thus we can expect the branching ratios for $\eta_{\psi,S} \rightarrow \gamma\gamma$ to be suppressed by $O(e/2)^4 \sim 10^{-3}$, and the monophoton signal becomes potentially more important for constraining the invisible decays of $\eta_{\psi,S}$ to dark matter. However we found in fig. 13(b) that in fact this constraint is also weak and does not yet restrict the model.

9.3 s -channel regime

As we discussed in sect. 2.3, both of the models considered here encompass an alternate picture for explaining the 130 GeV line, when the η_S or η_ψ meson has mass close to 260 GeV, due to the resonant annihilation $\chi\chi \rightarrow \eta \rightarrow 2\gamma$. In the case of the loop model, this is just another way of viewing the loop when it is resonantly enhanced, giving results that are compatible with the perturbative analysis. In the magnetic model however it is a qualitatively different mechanism, that does not rely upon the transition magnetic moment of the dark matter states. One can consider larger values of m_ψ that mildly suppress the magnetic moment, and allow the confinement scale to be smaller so that η_ψ gets most of its mass from the ψ constituents. However m_ψ cannot exceed 130 GeV, so quantitatively this regime is not far separated from the one previously considered. In any case, the LHC constraints are not more difficult to satisfy in this scenario, and it comes with the added prediction that the diphotons produced in 4-photon events should have invariant masses near 260 GeV. This is in the range we estimated to be reachable during the next LHC run.

9.4 Beyond 130 GeV

In case the 130 GeV line is not confirmed in future data, it is interesting to consider the implications of LHC constraints for possible future candidates of photophilic dark matter, which could produce a gamma ray line at some different energy. To illustrate the possibilities, we suppose that such a candidate is lurking just beyond the reach of Fermi's current sensitivity. The boundary of the 95%

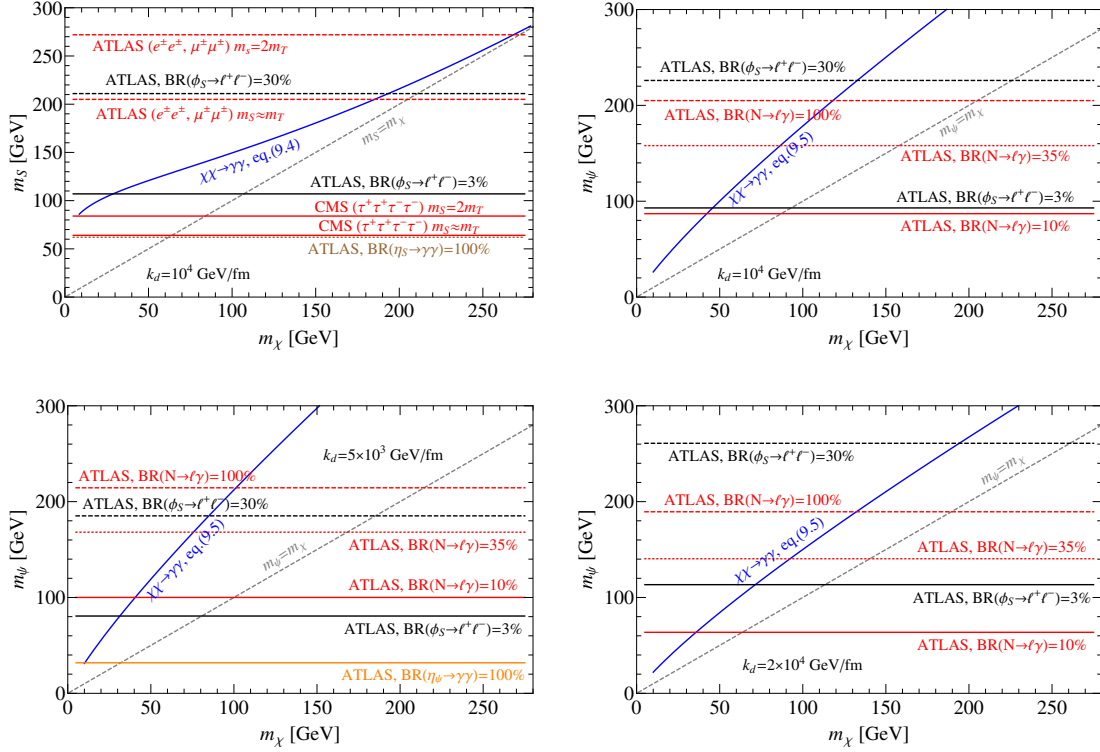


Figure 16. Summary of the LHC constraints on loop model and on MDM with various string tensions. (a) (upper left): loop model with string tension $k_d = 10^4$ GeV/fm; (b) (upper right): MDM with string tension $k_d = 10^4$ GeV/fm; (c) (lower left): MDM with string tension $k_d = 5 \times 10^3$ GeV/fm; (d) (lower right): MDM with string tension $k_d = 2 \times 10^4$ GeV/fm.

C.L. region found in ref. [8] (fig. 9, Einasto profile) is approximately given by

$$\langle \sigma v \rangle_{\max} \cong 0.03 \left(\frac{m_\chi}{100 \text{ GeV}} \right)^{4/3} \langle \sigma v \rangle_0 \quad (9.3)$$

(Recall that $\langle \sigma v \rangle_0 \equiv 1 \text{ pb} \cdot c$). By using this value in eqs. (2.2, 2.4) rather than the target value of $0.1 \langle \sigma v \rangle_0$ that we took in the case of 130 GeV DM, we obtain constraints on other parameters of the models as a function of m_χ , which imply the saturation of the current Fermi bound on the cross section. For the loop model, taking fiducial values $q = 2$, $N_c = 3$, $\lambda_{S\chi} = 3$ for the parameters other than m_s , and recalling that $r \equiv m_s/m_\chi$, the constraint reads

$$r^{-4} f(r) = 0.36 (m_\chi/100 \text{ GeV})^{10/3} \quad (9.4)$$

in the region $m_\chi \lesssim 300$ GeV. The solution of this transcendental equation is roughly fit by the linear relation $m_s = 84.5 + 0.67 m_\chi$. (For higher values of m_χ , the fine-tuned resonance condition $m_s \cong m_\chi$ needs to be satisfied to better than 1 part in 100 in order to get such a large cross section, while at $m_\chi \cong 100$ GeV, the tuning is only 50%.) The LHC constraints on the doubly charged scalar mass m_s for the case $k_d = 10^4$ GeV/fm are given in the first panel figure of fig. 16. The strongest

constraints come from the same-sign dileptons in the $e^\pm e^\pm$ or $\mu^\pm \mu^\pm$ channel and also the opposite-sign dilepton in the s-channel vector boson production. From these LHC final states, $m_s \lesssim (200 - 270)$ GeV is excluded if $m_s/2 \lesssim m_T \lesssim m_s$ and $\text{BR}(\phi_s \rightarrow \ell^+ \ell^-) = 30\%$. However, these constraints get significantly relaxed if η_{ST} decays into $\tau\tau$ dominantly and ϕ_s decays into η_S or η_T dominantly, as discussed before. Taking $\text{BR}(\phi_s \rightarrow \ell^+ \ell^-) = 3\%$, the scalar mass $m_s \lesssim 110$ GeV is excluded, which corresponds to dark matter mass around 30 GeV in the loop model. The CMS constraints on τ lepton final states are $m_s \gtrsim (60 - 80)$ GeV if $m_s/2 \lesssim m_T \lesssim m_s$.

Similarly for the magnetic dipole model, in the fiducial case of maximal mixing ($\cos\theta = 1$; see appendix C of [25]), and taking $m_\eta \cong \Lambda_d$, we can express m_ψ as a function of m_χ and Λ_d :

$$m_\psi = m_\chi^{5/6} \Lambda_d^{-1/2} \quad (9.5)$$

where all mass scales are in units of 100 GeV. The LHC constraints on the fermion mass m_ψ in MDM are shown in fig. 16 with three different values of the string tension, $k_d = (0.5, 1, 2) \times 10^4$ GeV/fm. For the opposite-sign dilepton channel with $\text{BR}(\phi_s \rightarrow \ell^+ \ell^-) = 3\%$, we have $m_\psi \gtrsim (80, 90, 110)$ GeV for $k_d = (0.5, 1, 2) \times 10^4$ GeV/fm respectively. Assuming equal branching ratios into all lepton flavors, the excited lepton search respectively constrains $m_\psi \gtrsim (170, 160, 140)$ GeV for the preceding values of k_d , corresponding to dark matter masses $m_\chi \sim (77, 88, 92)$ GeV.

10 Conclusion

We have presented constraints on two kinds of photophilic dark matter models that are capable of producing monoenergetic gamma rays in their annihilations, with energies $\gtrsim 100$ GeV. Our motivation is the tentative evidence for 130 GeV gamma rays from the galactic center, but of course such models could be of interest for future observations of monoenergetic photons at other energies. Both models require new charged scalars that are also strongly interacting under an unbroken $\text{SU}(N)_d$ (d for “dark”) gauge symmetry. The fact that any such particles that are pair-produced at LHC must “hadronize” to form $\text{SU}(N)_d$ -neutral mesonic (or baryonic) states is an essential feature in determining the constraints on producing such bound states, either singly or in pairs. These constraints arise from the decays of single vector “mesons” into lepton pairs, or from decays of two scalar mesons into two photon pairs.

A further common feature of the models is that, since any new charged state must be unstable, there exist couplings that allow them to decay into right-handed leptons, the simplest possibility amongst standard model particles that is allowed by gauge symmetry. In one of the models, this results in decays of charged mesons to like-sign lepton pairs, while in the other the decay is into a single lepton plus a photon. Both channels have been searched for by ATLAS and CMS.

The main conclusion of our study is that features of the models complementary to the ones most relevant for galactic 130 GeV gamma rays are constrained by the LHC data. One of the most important such parameters is the confinement scale Λ_d of the hidden $\text{SU}(N)_d$ gauge group, which sets the scale of the exotic meson masses if Λ_d is greater than the masses of the constituent particles. In general, we find that Λ_d must not be small compared to the constituent masses in order to avoid LHC constraints on the meson masses. For example, if the vector meson ϕ_s is not far above 310 GeV, it should be seen in the next run of the LHC. Since $m_s = 130 - 148$ GeV to explain the 130 GeV line in the loop model, ϕ_s should get a significant fraction of its mass from the dark sector gluons. However Λ_d also cannot be much larger than m_s in this model, since the complementary description of the gamma ray line production in terms of bound state decays into photons, eq. (2.9), shows that some degree of resonant enhancement is required. In the magnetic dark matter model on the other hand, there

LHC Observable	Constraint (loop model)	Constraint (MD model)
same-sign dileptons	$\text{BR}(\eta_{ST} \rightarrow ee, \mu\mu) \ll 1$ or $m_{\eta_{ST}} > 200 \text{ GeV}$	–
vector meson production	$m_{\phi_S} > 310 \text{ GeV}$ $\Lambda_d > \text{few} \times m_S$	$m_{\phi_\psi} > 250 \text{ GeV}$ $\Lambda_d \gtrsim 300 \text{ GeV}$
excited lepton searches	–	$m_N > 370 \text{ GeV}$
diphoton production	$m_{\eta_S} > 220 \text{ GeV}$	$m_{\eta_\psi} > 140 \text{ GeV}$
4-photon events (14 TeV, 100 fb ⁻¹)	$m_{\eta_S} > 750 \text{ GeV}$	$m_{\eta_\psi} > 600 \text{ GeV}$
monophotons	–	–

Table 2. Summary of LHC constraints found for the loop model and the magnetic dipole model for 130 GeV dark matter. The 4-photon constraints are projected, based on the ultimate reach of LHC.

is no strong prohibition against taking Λ_d large in order to give the observed 130 GeV line, but an accidental cancellation is needed to make $m_\chi = 130 \text{ GeV}$ if Λ_d is much greater than m_χ . We provide a summary of our results (subject to assumptions about values of other parameters, as discussed in the text) in table 2.

It is possible that either model will be discovered by exotic signatures: $\eta_{ST} \rightarrow \ell^+ \ell^+$ (same-sign dileptons) in the loop model, or $N^- \rightarrow \ell^- \gamma$ in the magnetic model. In the former case, this depends upon assumptions about the flavor structure of the dimension-5 operator $\Lambda_{ij}^{-1} S T^* \bar{l}_{R,i}^c l_{R,j}$. The limits or discovery potential are stronger if the couplings to e or μ dominate. Interestingly, the constraint from $N^- \rightarrow \ell^- \gamma$ is less sensitive to hierarchies in the flavor structure of the relevant coupling $y_i \epsilon_{ab} S_a^* \bar{l}_{R,i} \psi_b$ because the resulting effective interaction is due to transition magnetic moments that are inversely proportional to the lepton mass (but proportional to y_i). In the minimally flavor violating case we get a limit of $m_{N^-} \gtrsim 370 \text{ GeV}$.

If the 130 GeV line does not persist as data improves, our results may be of interest in case of future anomalies of this type. It would be straightforward to generalize the analysis given here for gamma ray lines at higher energies. We took a first step in this direction in section 9.4. We believe the models considered here incorporate several generic features that are useful for obtaining strong gamma ray lines from dark matter annihilation, namely, the existence of new charged scalars and a new confining gauge interaction.

One of the main uncertainties in our treatment was in the prediction of hadronic matrix elements and bound state masses, involving the dark $\text{SU}(N)_d$ gauge sector. We used a rather crude model for predicting these quantities, rescaling with reference to QCD. If the scenarios presented here become more motivated by future experimental results, it would be worthwhile to study these properties within lattice gauge theory to obtain more accurate predictions.

Acknowledgments. We thank Baris Altunkaynak, David Berge, Ning Chen, Guy Moore and Mike Trott for helpful discussions. JC thanks the University of Jyväskylä Department of Physics for its hospitality during the completion of this work. Our research is supported by the Natural Sciences and Engineering Research Council (NSERC) of Canada.

A Amplitude for photoproduction of ϕ_s

Section 5.3 of ref. [34] derives the amplitude for photoproduction of vector mesons in QCD leading to the result (5.3). This must be modified for bound states with orbital angular momentum, for which the wave function vanishes at the origin. The general relation for the amplitude of $q\bar{q} \rightarrow \phi_s$, from eq. (5.44) of [34], is

$$\mathcal{M}(q\bar{q} \rightarrow \phi_s) = \frac{\sqrt{2m_{\phi_s}}}{2E_s} \int \frac{d^3k}{(2\pi)^3} \tilde{\psi}^*(\vec{k}) \mathcal{M}(q\bar{q} \rightarrow SS^*) \quad (\text{A.1})$$

where $\tilde{\psi}(k)$ is the wave function of S in momentum space. In the limit where S is nonrelativistic, the matrix element for $q\bar{q} \rightarrow SS^*$ is given by $(2e^2 q_q q_s / s) \bar{v}_{\bar{q}} \vec{k} \cdot \vec{\gamma} u_q$, so (A.1) becomes

$$\mathcal{M}(q\bar{q} \rightarrow \phi_s) = \frac{e^2 q_q q_s \sqrt{2m_{\phi_s}}}{s E_s} \bar{v}_{\bar{q}} \vec{\gamma} u_q \cdot \vec{\nabla} \psi^*(0) \quad (\text{A.2})$$

Taking the quarks to be relativistic and averaging over their spins and directions, one finds

$$\langle |\mathcal{M}(q\bar{q} \rightarrow \phi_s)|^2 \rangle = 2 \frac{e^4 q_q^2 q_s^2 m_{\phi_s}}{3 s E_s^2} |\vec{\nabla} \psi(0)|^2 \quad (\text{A.3})$$

The same amplitude can be used for $\phi_s \rightarrow e^+ e^-$ by replacing $q_q \rightarrow 1$ and multiplying by 4 to remove the averaging over fermion spins. (There is no need to average over polarizations of ϕ_s since by holding $\vec{\nabla} \psi(0)$ fixed we effectively choose a single polarization.) Then by computing the decay rate in the usual way, we arrive at (5.4).

B “Bohr model” of exotic mesons

To estimate masses of bound states in our models, we use a semiclassical quantization approach for a linear confining potential of the form $V = 2k_d r$, where k_d is the string tension of the $SU(N)_d$ force, with constituents whose mass is m and separation is $2r$. In the nonrelativistic case, the energy of the bound state is $p^2/m + V$. Following Bohr we consider circular orbits of radius r and demand that the angular momentum $L = 2pr$ be quantized, $L = n$. In this way the bound state energy becomes $2m + n^2/(4r^2m) + 2k_d r$, which is minimized at $r_n = (n/2)^{2/3} (mk_d)^{-1/3}$, $p_n = (nk_d m/2)^{1/3}$, $E_n = 2m + 3(nk_d/2)^{2/3} m^{-1/3}$. For the relativistic case, the energy becomes $2\sqrt{p^2 + m^2} + 2kr$, again with $2pr = n$, leading to a cubic equation for p^2 . If $p \gg m$ it simplifies to $p = \sqrt{nk/2}$, $E = 2\sqrt{2nk}$. This model ignores spin-spin interactions and therefore does not give very accurate predictions for QCD mesons, but may be more suitable for the η_s and ϕ_s mesons of the dark matter models, where S is spin-zero. In the spirit of the Bohr approach these are assigned quantum numbers of $n = 1$ and $n = 2$ respectively, even though their angular momenta are lower by one unit.

References

- [1] T. Bringmann, X. Huang, A. Ibarra, S. Vogl and C. Weniger, JCAP **1207**, 054 (2012) [arXiv:1203.1312 [hep-ph]].
- [2] C. Weniger, JCAP **1208**, 007 (2012) [arXiv:1204.2797 [hep-ph]].
- [3] E. Tempel, A. Hektor and M. Raidal, JCAP **1209**, 032 (2012) [Addendum-ibid. **1211**, A01 (2012)] [arXiv:1205.1045 [hep-ph]].
- [4] M. Su and D. P. Finkbeiner, arXiv:1206.1616 [astro-ph.HE].

- [5] A. Hektor, M. Raidal and E. Tempel, arXiv:1209.4548 [astro-ph.HE].
- [6] D. P. Finkbeiner, M. Su and C. Weniger, JCAP **1301**, 029 (2013) [arXiv:1209.4562 [astro-ph.HE]].
- [7] E. Carlson, T. Linden, S. Profumo and C. Weniger, arXiv:1304.5524 [astro-ph.HE].
- [8] [Fermi-LAT Collaboration], arXiv:1305.5597 [astro-ph.HE].
- [9] A. Hektor, M. Raidal and E. Tempel, Astrophys. J. **762**, L22 (2013) [arXiv:1207.4466 [astro-ph.HE]].
- [10] M. Su and D. P. Finkbeiner, arXiv:1207.7060 [astro-ph.HE].
- [11] M. Ackermann *et al.* [LAT Collaboration], Phys. Rev. D **86**, 022002 (2012) [arXiv:1205.2739 [astro-ph.HE]].
- [12] D. P. Finkbeiner, M. Su and C. Weniger, JCAP **1301**, 029 (2013) [arXiv:1209.4562 [astro-ph.HE]].
- [13] A. Hektor, M. Raidal and E. Tempel, arXiv:1209.4548 [astro-ph.HE].
- [14] Y. Bai, M. Su and Y. Zhao, arXiv:1212.0864 [hep-ph].
- [15] Y. Zhang, arXiv:1212.2730 [hep-ph].
- [16] H. M. Lee, M. Park and V. Sanz, arXiv:1212.5647 [hep-ph].
- [17] J. Kopp, E. T. Neil, R. Primulando and J. Zupan, arXiv:1301.1683 [hep-ph].
- [18] J. Fan and M. Reece, arXiv:1301.2597 [hep-ph].
- [19] N. Zhou, D. Berge and D. Whiteson, arXiv:1302.3619 [hep-ex].
- [20] J. Liu, B. Shuve, N. Weiner, I. Yavin arXiv:1303.4404 [hep-ph].
- [21] F. Domingo, O. Lebedev, Y. Mambrini, J. Quevillon, A. Ringwald, arXiv:1305.6815 [hep-ph].
- [22] J. M. Cline, Phys. Rev. D **86**, 015016 (2012) [arXiv:1205.2688 [hep-ph]].
- [23] M. R. Buckley and D. Hooper, Phys. Rev. D **86**, 043524 (2012) [arXiv:1205.6811 [hep-ph]].
- [24] F. D’Eramo, M. McCullough and J. Thaler, JCAP **1304**, 030 (2013) [arXiv:1210.7817 [hep-ph]].
- [25] J. M. Cline, G. D. Moore and A. R. Frey, Phys. Rev. D **86**, 115013 (2012) [arXiv:1208.2685 [hep-ph]].
- [26] N. Weiner and I. Yavin, Phys. Rev. D **87**, 023523 (2013) [arXiv:1209.1093 [hep-ph]].
- [27] G. Hinshaw *et al.* [WMAP Collaboration], arXiv:1212.5226 [astro-ph.CO].
- [28] T. E. O. Ericson, B. Loiseau and A. W. Thomas, Phys. Rev. C **66**, 014005 (2002) [hep-ph/0009312].
- [29] W. Ochs, J. Phys. G **40**, 043001 (2013) [arXiv:1301.5183 [hep-ph]].
- [30] M. Muhlleitner and M. Spira, Phys. Rev. D **68**, 117701 (2003) [hep-ph/0305288].
- [31] S. Chatrchyan *et al.* [CMS Collaboration], Eur. Phys. J. C **72**, 2189 (2012) [arXiv:1207.2666 [hep-ex]].
- [32] G. Aad *et al.* [ATLAS Collaboration], arXiv:1210.5070 [hep-ex].
- [33] M. Ciuchini, G. Degrossi, P. Gambino and G. F. Giudice, Nucl. Phys. B **534**, 3 (1998) [hep-ph/9806308].
- [34] M. E. Peskin and D. V. Schroeder, Reading, USA: Addison-Wesley (1995) 842 p
- [35] [ATLAS Collaboration], ATLAS-CONF-2013-017.
- [36] [CMS Collaboration], CMS PAS EXO-12-061.
- [37] [ATLAS Collaboration], ATLAS-CONF-2012-008.
- [38] [ATLAS Collaboration], ATLAS-CONF-2012-087.

- [39] S. Chatrchyan *et al.* [CMS Collaboration], Phys. Rev. Lett. **108**, 111801 (2012) [arXiv:1112.0688 [hep-ex]].
- [40] [ATLAS Collaboration], ATLAS-CONF-2013-012.
- [41] [CMS Collaboration], CMS-PAS-HIG-13-001.
- [42] J. Alwall, P. Demin, S. de Visscher, R. Frederix, M. Herquet, F. Maltoni, T. Plehn and D. L. Rainwater *et al.*, JHEP **0709**, 028 (2007) [arXiv:0706.2334 [hep-ph]].
- [43] T. Sjostrand, S. Mrenna and P. Z. Skands, JHEP **0605**, 026 (2006) [hep-ph/0603175].
- [44] J. Conway *et al.*, “PGS 4: Pretty Good Simulation of high energy collisions,” 2006, <http://www.physics.ucdavis.edu/~conway/research/software/pgs/pgs4-general.htm>.
- [45] G. Aad *et al.* [ATLAS Collaboration], arXiv:0901.0512 [hep-ex].
- [46] J. Alwall, M. Herquet, F. Maltoni, O. Mattelaer and T. Stelzer, JHEP **1106**, 128 (2011) [arXiv:1106.0522 [hep-ph]].
- [47] [ATLAS Collaboration], ATL-PHYS-PUB-2011-007.
- [48] G. Aad *et al.* [ATLAS Collaboration], JHEP **1301**, 086 (2013) [arXiv:1211.1913 [hep-ex]].
- [49] J. G. Korner, J. H. Kuhn, M. Krammer and H. Schneider, Nucl. Phys. B **229**, 115 (1983).
- [50] S. Chatrchyan *et al.* [CMS Collaboration], Phys. Rev. Lett. **108**, 261803 (2012) [arXiv:1204.0821 [hep-ex]].
- [51] S. Chatrchyan *et al.* [CMS Collaboration], JHEP **1209**, 094 (2012) [arXiv:1206.5663 [hep-ex]].
- [52] G. Aad *et al.* [ATLAS Collaboration], arXiv:1209.4625 [hep-ex].